**รายงานวิจัยฉบับสมบูรณ์**

# โครงการ: โครงสร้างและหน้าที่ของโปรตีนชนิดใหม่ที่ตอบสนองต่อการติดเชื้อไวรัสจากกุ้งกุลาดำ *Penaeus monodon*, *Pm*VRP15

**โดย ผู้ช่วยศาสตราจารย์ ดร. เกื้อการุณย์ ครูส่ง และคณะ**

**กันยายน 2558**

**สัญญาเลขที่** RSA 5580053

**รายงานวิจัยฉบับสมบูรณ์**

# โครงการ: โครงสร้างและหน้าที่ของโปรตีนชนิดใหม่ที่ตอบสนองต่อการติดเชื้อไวรัสจากกุ้งกุลาดำ *Penaeus monodon*, *Pm*VRP15

**คณะผู้วิจัย**

**1. หัวหน้าโครงการวิจัยผู้รับทุน : ผู้ช่วยศาสตราจารย์ ดร. เกื้อการุณย์ ครูส่ง**

**ศูนย์เชี่ยวชาญเฉพาะทางด้านอณูชีววิทยาและจีโนมกุ้ง ภาควิชาชีวเคมี คณะวิทยาศาสตร์ จุฬาลงกรณ์มหาวิทยาลัย**

**2. นักวิจัยที่ปรึกษา : ศาสตราจารย์ ดร. อัญชลี ทัศนาขจร**

**ศูนย์เชี่ยวชาญเฉพาะทางด้านอณูชีววิทยาและจีโนมกุ้ง ภาควิชาชีวเคมี คณะวิทยาศาสตร์ จุฬาลงกรณ์มหาวิทยาลัย**

สนับสนุนโดยสำนักงานคณะกรรมการอุดมศึกษา และสำนักงานกองทุนสนับสนุนการวิจัย

(ความเห็นในรายงานนี้เป็นของผู้วิจัย สกอ. และ สกว.ไม่จำเป็นต้องเห็นด้วยเสมอไป)

**กิตติกรรมประกาศ**

ผู้วิจัยขอขอบคุณ ศาสตราจารย์ ดร. อัญชลี ทัศนาขจร และ ดร. เปรมฤทัย สุพรรณกูล ศูนย์เชี่ยวชาญเฉพาะทางด้านอณูชีววิทยาและจีโนมกุ้ง ภาควิชาชีวเคมี คณะวิทยาศาสตร์ จุฬาลงกรณ์มหาวิทยาลัย ที่ได้ให้คำปรึกษาและคำแนะนำที่เป็นประโยชน์ต่อโครงการวิจัยนี้

โครงการวิจัยนี้ได้รับทุนสนับสนุนจากสำนักงานคณะกรรมการอุดมศึกษา สำนักงานกองทุนสนับสนุนการวิจัย จุฬาลงกรณ์มหาวิทยาลัย และทุนวิจัยบางส่วนจากกองทุนรัชดาภิเษกสมโภช จุฬาลงกรณ์มหาวิทยาลัย

**บทคัดย่อ**

---

**(Thai) โครงสร้างและหน้าที่ของโปรตีนชนิดใหม่ที่ตอบสนองต่อการติดเชื้อไวรัสจากกุ้งกุลาดำ *Penaeus monodon*, *Pm*VRP15**

---

งานวิจัย suppression subtractive hybridization library ค้นพบยีน viral responsive protein 15 (*Pm*VRP15) ที่มีการแสดงออกเพิ่มสูงขึ้นมากกว่า 9,000 เท่า ในเซลล์เม็ดเลือดของกุ้งกุลาดำที่ติดเชื้อไวรัสตัวแดงดวงขาว (white spot syndrome virus, WSSV) ที่ 48 ชั่วโมง (Vatanavicharn et al., 2014) ผลการยับยั้งการแสดงออกของยีน *Pm*VRP15 ด้วยเทคนิค RNA interference พบว่า เมื่อฉีด dsRNA *Pm*VRP15 ส่งผลให้อัตราการเพิ่มจำนวนของไวรัส ลดลง เมื่อเปรียบเทียบกับกลุ่มควบคุม จึงกล่าวได้ว่า ยีน *Pm*VRP15 มีผลต่อการเพิ่มจำนวนของไวรัสตัวแดงดวงขาว เมื่อวิเคราะห์การแสดงออกของโปรตีน *Pm*VRP15 ด้วย confocal laser scanning microscope พบว่า โปรตีน *Pm*VRP15 มีการแสดงออกบริเวณนิวเคลียร์เมมเบรน ซึ่งจากการทำนายโครงสร้างของโปรตีนดังกล่าว พบว่า *Pm*VRP15 ประกอบด้วย transmembrane อยู่ 1 ส่วน เมื่อสกัดแยกเซลล์เม็ดเลือดของกุ้งกุลาดำที่ติดเชื้อไวรัสตัวแดงดวงขาวเป็นแต่ละส่วน (subcellular fractionation) จะพบโปรตีน *Pm*VRP15 อยู่ในส่วนใสของนิวเคลียส และส่วนที่จับกับโครมาติน ดังนั้น *Pm*VRP15 อาจเกี่ยวข้องกับการเข้าสู่นิวเคลียสหรือการออกจากนิวเคลียสของไวรัสตัวแดงดวงขาว เพื่อทดสอบสมมติฐานดังกล่าว จึงทำการตรวจวัดปริมาณไวรัสในส่วนของนิวเคลียสและไซโทพลาสซึมในสภาวะที่ยับยั้งการแสดงออกของยีน *Pm*VRP15 เทียบกับกลุ่มควบคุม ซึ่งพบว่า การยับยั้งการแสดงออกของยีน *Pm*VRP15 ส่งผลให้จำนวนไวรัสตัวแดงดวงขาวในส่วนนิวเคลียสต่อไซโทพลาสซึมลดลงกว่ากลุ่มควบคุมถึง 9.3 เท่า จึงคาดว่า *Pm*VRP15 น่าจะเกี่ยวข้องกับการเข้าสู่นิวเคลียสของไวรัสตัวแดงดวงขาว เมื่อนำรีคอมบิแนนท์โปรตีน *Pm*VRP15 ที่ผลิตใน *Escherichia coli* C43 (DE3) มาทำให้บริสุทธิ์ด้วยคอลัมน์ Ni-NTA and DEAE Sepharose แล้วนำไปหา circular dichroism spectra พบว่ารีคอมบิแนนท์ *Pm*VRP15 ประกอบด้วยส่วนของแอลฟาฮีลิกซ์ 48% และบีต้าชีท 14% การวิเคราะห์รีคอมบิแนนท์ *Pm*VRP15 ด้วยเทคนิค analytical ultracentrifugation พบว่า *Pm*VRP15 สามารถจับกันเป็นเตตระเมอร์ (tetramer) ที่ความเข้มข้นโปรตีน 60 μM นอกจากนี้ ได้ทำการทดลอง หาสภาวะที่เหมาะสมในการตกผลึก *Pm*VRP15 ใน 96-well plate แต่ไม่พบสภาวะที่ทำให้เกิดผลึกโปรตีนที่มีการเลี้ยวเบนรังสีเอ็กซ์ที่ดี

**คำหลัก:** *Penaeus monodon*, viral responsive protein 15, white spot syndrome virus, WSSV

## Abstract

**(English)** **Structure and Function of a Novel Responsive Protein from the Black Tiger Shrimp *Penaeus monodon, Pm*VRP15**

A viral responsive protein 15 (*Pm*VRP15) was previously identified from suppression subtractive hybridization library. *Pm*VRP15 was highly up-regulated (> 9000 folds at 48 hours) after WSSV challenge (Vatanavicharn et al., 2014). Double-stranded RNAi-mediated knockdown of *Pm*VRP15 gene expression suggested that *Pm*VRP15 has a crucial role in WSSV propagation in *P. monodon*. Confocal laser scanning microscopy showed that *Pm*VRP15 localized around the nuclear membrane of shrimp hemocytes. Analysis of *Pm*VRP15 sequence predicted that *Pm*VRP15 possesses one transmembrane segment. Subcellular fractionation study showed that *Pm*VRP15 was found in soluble nuclear and chromatin-bound fractions. As a result, *Pm*VRP15 may function in a nucleus and involve in nuclear import/export of WSSV. To test this hypothesis, ratio of WSSV DNA in nuclear and cytoplasmic fractions of *Pm*VRP15-silenced hemocytes was compared to that of the control. *Pm*VRP15 silencing resulted in a lower ratio of WSSV copy number (9.3 fold) in nuclear and cytoplasmic fractions, indicating that *Pm*VRP15 may play a role in nuclear entry of WSSV. For structural study, recombinant *Pm*VRP15 was expressed in *Escherichia coli* C43 (DE3) and purified by Ni-NTA and DEAE Sepharose columns. Circular dichroism spectra showed that *Pm*VRP15 contains 48% of alpha-helix and 14% of beta-sheet. Analytical ultracentrifugation study suggested that *Pm*VRP15 forms a tetramer at 60 μM. Crystallization screening of *Pm*VRP15 was performed in 96-well plate using several crystallization screens. However, no good diffracted protein crystal was obtained.

**Keywords:** *Penaeus monodon*, viral responsive protein 15, white spot syndrome virus, WSSV

## Executive Summary

---

**(English)** **Structure and Function of a Novel Responsive Protein from the Black Tiger Shrimp *Penaeus monodon, Pm*VRP15**

**(Thai)** **โครงสร้างและหน้าที่ของโปรตีนชนิดใหม่ที่ตอบสนองต่อการติดเชื้อไวรัสจากกุ้งกุลาดำ *Penaeus monodon*, *Pm*VRP15**

---

### 1. Introduction to the research problem and its significance

Thailand is the world's largest shrimp exporter. Each year shrimp export has brought in 80-100 billion baht in revenue. The Thai shrimp industries are expected to grow as demand on international markets is rising. However, contrary to market expectations, the black tiger shrimp export volume has dropped dramatically since 2002. Export value of the black tiger shrimp fell down over 10 times from 28,299.90 million baht in 2002 to 1,879.64 million baht in 2014 (http://www.oae.go.th/oae-report/export_import/export_result.php). This reflects the fact that Thai shrimp industries have shifted from the black tiger shrimp *Penaeus monodon* to the white shrimp *Litopenaeus vannamei* and the black tiger shrimp farming is under a prominent threat of extinction. The demand of the black tiger shrimp in oversea markets remains high and command high price. However, its low survival rate and high production cost make Thai shrimp farmers switch to the white shrimp.

Outbreaks of shrimp viruses *e.g.* yellow head virus (YHV) and white spot syndrome virus (WSSV) cause catastrophic losses in shrimp industry. WSSV is highly infectious and white spot syndrome (WSS) can cause 100% mortality of farmed shrimp within a few days. Despite the fact that WSSV is a devastating threat to shrimp aquaculture, the mechanism of WSSV infection has not yet been fully understood. Suppression subtractive cDNA libraries of *P. monodon* have revealed a novel viral responsive protein, namely *Pm*VRP15. This unknown protein was highly up-regulated in response to WSSV infection. *Pm*VRP15 was highly expressed in haemocyte, gill, heart and lymphoid tissues. Immunofluorescence showed that *Pm*VRP15 localized at the nuclear envelope of infected shrimp's haemocytes. Double-stranded RNAi-mediated knockdown of *Pm*VRP15 gene expression suggested that

*Pm*VRP15 has a role in WSSV propagation in shrimps (Vatanavicharn et al, 2014). This work aims to examine roles of *Pm*VRP15 in nuclear entry and export of WSSV and investigate the structure of *Pm*VRP15. As a result, this research could gain insights into the molecular mechanism between WSSV and host interaction; and also promote our understanding of the virus control.

**2. Objectives**

2.1 To investigate effect of *Pm*VRP15 gene silencing on WSSV infection *in vitro*

2.2 To study localization of *Pm*VRP15

2.3 To study roles of *Pm*VRP15 in nuclear import and export of WSSV

2.4 To produce and characterize the recombinant *Pm*VRP15

2.5 To crystallize *Pm*VRP15

**3. Research Methodology**

**3.1 *Pm*VRP15 mRNA expression in response to WSSV infection in shrimp hemocyte primary cell culture**

Primary hemocyte cultures of $10^6$ cells per ml were treated with 400 µl of fresh L-15 culture medium either with or without 50 µl of the diluted WSSV solution (~15,000 viral copies/µl). Hemocyte cultures were then incubated at 28 °C and total RNA was extracted from the hemocytes at 0, 6, 12, 24, 48 and 72 h post-WSSV infection using the TRI Reagent® (Molecular Research Center) followed by DNase I, RNase-free (Thermo scientific) treatment, and used for single-stranded cDNA synthesis by the First Strand cDNA Synthesis Kit (Thermo Scientific). The transcription level of target genes was identified by RT-PCR using an equal amount of cDNA template with gene-specific primers (Table 1). The Elongation factor-1 alpha (EF-1$\alpha$) was used as an internal control. The PCR conditions consisted of 94 °C for 3 min, followed by 33 cycles (for *Pm*VRP15) or 28 cycles (for EF-1$\alpha$) cycles of 95 °C for 30 sec, 58 °C for 30 sec and 72 °C for 30 sec, and a final extension at 72 °C for 5 min. The PCR products were analyzed by 1.5% (w/v) agarose gel electrophoresis and visualized using Gel

Documentation System (Syngene). The differential expression level of VRP15 was reported as relative to EF-1α.

**Table 1** Nucleotide sequences of primers for RT-PCR amplification

| Primer | Sequence (5´-3´) |
|---|---|
| *ie1*-FRT | GACTCTACAAATCTCTTTGCCA |
| *ie1*-RRT | CTACCTTTGCACCAATTGCTAG |
| VP28-FRT | TCACTCTTTCGGTCGTGTCG |
| VP28-RRT | CCACACACAAAGGTGCCAAC |
| *Pm*VRP15-RTF | CGATCACCACTCTCGTTCTT |
| *Pm*VRP15-RTR | ACAGCGACTCCAAGGTCTACGA |

The expression level of *Pm*VRP15 and EF-1α gene was further analyzed by quantitative real time RT-PCR (qRT-PCR) using specific primers as shown in Table 2. The reaction volume of 10 µl contained 5 µl of 2X SsoFast™ EvaGreen® Supermix (Bio-Rad), 0.5 µM of each forward and reverse primers, and 1 µl of 1:3 diluted cDNA template. A negative control reaction contained no cDNA template. The qRT-PCR was performed using the CFX96™ Real-Time PCR Detection System (Bio-Rad). The PCR condition was performed as follows: 95 °C for 30 sec, followed by 40 cycles of 95 °C for 5 sec, 58 °C for 5 sec and 60 °C for 5 sec. The experiment was carried out in triplicate. The threshold cycle ($C_T$) for each sample was analyzed by a mathematical model (Pfaffl, 2001). The data were shown as means ± standard deviations (SD). Statistical analysis was done using the one-way ANOVA followed by post hoc test (Duncan's new multiple range test). Data differences were considered significant at $P < 0.05$ (*), $P < 0.01$ (**).

**Table 2** Nucleotide sequences of primers for qRT-PCR amplification

| Primer | Sequence (5´-3´) |
|---|---|
| EF1-α QF | GGTGCTGGACAAGCTGAAGGC |
| EF1-α QR | CGTTCCGGTGATCATGTTCTTGATG |
| VP28QF | GGGAACATTCAAGGTGTGGA |
| VP28QR | GGTGAAGGAGGAGGTGTTGG |
| *Pm*VRP15-QF | CGTCCTTCAGTGCGCTTCCATA |
| *Pm*VRP15-QR | ACAGCGACTCCAAGGTCTACGA |

**3.2 Effects of *Pm*VRP15-silencing on WSSV infection in shrimp hemocyte primary cell culture**

The hemocyte cell cultures ($10^6$ cells per ml per well) were divided into 3 groups and incubated with either 50 µl of L-15 medium (Group 1) or 50 µl of L-15 medium with 20 µg/well of GFP dsRNA (Group 2) or 50 µl of L-15 medium with 20 µg/well of *Pm*VRP15 dsRNA (Group 3). After 12 h, 50 µl of L-15 medium with or without, GFP dsRNA (10 µg/well) and *Pm*VRP15 dsRNA (10 µg/well) were added along with 50 µl of diluted WSSV solution (~15,000 viral copies/µl) and incubated at 27 °C. At 24 h post-WSSV infection, hemocyte cells were harvested and total RNA was extracted from hemocytes using the TRI Reagent® (Molecular Research Center) followed by DNase I, RNase-free (Thermo scientific) treatment. Then, single-stranded cDNA was synthesized with the First Strand cDNA Synthesis Kit (Thermo Scientific) and cDNA was used to analyze VP28 mRNA expression by RT-PCR with EF-1α as an internal reference.

The expression levels of VP28, VRP15 and EF-1α genes were analyzed by RT-PCR and qRT-PCR as previously described in 3.1.

Comparative $C_T$ method was used to compare the gene expression in two different samples. The fold change of gene expression was calculated using following formula.

$$\text{Fold change} = 2^{-\Delta\Delta C_T}$$

$\Delta\Delta C_T$ = [($C_T$ gene of interest - $C_T$ internal control) sample A - ($C_T$ gene of interest - $C_T$ internal control) sample B)]

**3.3 Immunolocalization of *Pm*VRP15 and VP28 in normal and *Pm*VRP15-knockdown hemocytes infected by WSSV**

Twenty-five µl of 150 mM sodium chloride containing GFP dsRNA (5 µg/g shrimp) or *Pm*VRP15 dsRNA (10 µg/g shrimp) was injected into each shrimp (~10 g body weight). After 24 h, the shrimp were injected with 25 µl of 150 mM sodium chloride containing GFP dsRNA (5 µg/g shrimp) or *Pm*VRP15 dsRNA (5 µg/g shrimp), along with 30 µl of the diluted WSSV solution (~ 4 x$10^3$ viral copies). At 48 h post-injection, hemolymph was immediately fixed with of 4% (w/v) paraformaldehyde in PBS, pH 7.4 (ratio 1:1) and incubate at RT for 10 min. Hemocytes were collected by centrifugation at 800 x g for 10 min and washed three times with PBS, pH 7.4, and then immersed in PBS, pH 7.4, and kept at 4 °C until used.

Hemocytes were attached onto a polylysine coated microscope slide (Polysine slides, Thermo Scientific) using cytospin centrifugation. The slide was washed by PBS for 5 min and later covered by 200 µl of 0.1% (v/v) Triton-X 100 in PBS for 5 min at RT to permeabilize the hemocyte membrane. After rinsing the slide in PBS for 5 min, it was immersed in 200 µl of blocking solution (10% (v/v) FBS in PBS) for 1 h at RT followed by washing in PBS. The fixed hemocytes were incubated with a 1:500 dilution of purified rabbit anti-*Pm*VRP15 polyclonal antibody and 1:100 dilution of mouse anti-VP28 polyclonal antibody in PBS, pH 7.4, containing 1% (v/v) FBS at RT for 3 h. After PBS washing, the fixed hemocytes were incubated with a 1:500 dilution of Alexa Fluor 488 goat anti-rabbit IgG antibody (Invitrogen) and Alexa Fluor® 568 goat anti-mouse IgG antibody (Invitrogen) in PBS, pH 7.4 at RT for 1 h in the dark. The nucleus was then stained with a 1:1500 dilution of TO-PRO-3 iodide (Invitrogen) in PBS, pH 7.4, at RT for 10 min in the dark. The cover slips were then coated with

Prolong Gold Antifade Reagent (Invitrogen) and kept in dark at 4 °C until they were visualized under a confocal laser scanning microscope (Olympus).

**3.4 Protein localization of *Pm*VRP15 by subcellular protein fractionation**

The hemocyte cell cultures were incubated with 50 µl of the diluted WSSV solution (~15,000 viral copies/µl) and incubated at 27 °C. For 48 h post-WSSV infection, total protein was extracted from hemocytes using Subcellular fractionation kit for cultured cells (Thermo Scientific). Cytoplasmic, membrane, soluble nuclear, chromatin-bound and cytoskeletal fractions were extracted. The total protein concentration of each fraction was determined using BCA protein assay and 10 µg of proteins were loaded on to SDS-PAGE. Each fraction was probed with anti-*Pm*VRP15 as primary antibody (1:1000) at 37 °C for 3 h. After washing with PBST, membrane was probed with alkaline phosphatase-conjugated goat anti-rabbit IgG (1:10,000).

**3.5 Roles of *Pm*VRP15 in nuclear import and export of WSSV**

The hemocyte cell cultures were divided into 2 groups and incubated with 50 µl of either GFP dsRNA (20 µg/well) or VRP15 dsRNA (20 µg/well). After 12 h, 50 µl of GFP dsRNA (10 µg/well) or VRP15 dsRNA (10 µg/well) were added, along with 50 µl of the diluted WSSV solution (~15,000 viral copies/µl) and incubated at 27 °C. For 24 h post-WSSV infection, the cytoplasmic and nuclear fractions were separated by Subcellular fractionation kit for cultured cells (Thermo Scientific) and total DNA was extracted from each fraction. WSSV copy number in each fraction was then determined by Real-time PCR using WSSV1011F/WSSV1079R primers, as described by (Durand, 2002). The experiment was carried out in triplicate and WSSV recombinant plasmid (known copy number) was used as the standard for quantification.

To confirm that there is no cross-contamination between cytoplasmic and nuclear fractions, 10 µg of proteins from each fraction were applied on SDS-PAGE and anti-Nuclear Pore Complex (NPC) antibody (1:1000) was used as a primary antibody for Western blotting. Pierce™ Fast Western Blot Kit, SuperSignal™ West Femto was used for Western blot detection.

### 3.6 Expression of recombinant *Pm*VRP15 in *Saccharomyces cerevisiae* expression system

#### 3.6.1 Cloning of *Pm*VRP15 gene into pDDGFP2 vector by homologous recombination

*Pm*VRP15 gene was inserted into pDDGFP-2 vector, which has a GAL1 promoter and URA selection marker, by homologous recombination (Newstead et al, 2007). In brief, *Pm*VRP15 gene was amplified with *Pm*VRP15-F (5´-TCGACGGATTCTAGAACTAGTGGATCCC CC -3´) and *Pm*VRP15-R (5´-AAATTGACCTTGAAAATATAAATTTTCCCC -3´) primers that include 5' overhangs complementing the upstream and downstream sequences to either side of the *Sma* I site in pDDGFP-2 vector. PCR reaction was carried out by the following condition: an initial denaturation at 95 ℃ for 1 min, followed by 35 cycles of denaturation at 95 ℃ for 30 s, annealing at 60 ℃ for 30 s, elongation at 68 ℃ for 1 min, and the final extension at 68℃ for 10 min. PCR product was then mixed with *Sma* I-linearized pDDGFP-2 vector and transformed into *S. cerevisiae* competent cells.

#### 3.6.2 Expression of recombinant *Pm*VRP15 in *S. cerevisiae*

A colony of *S. cerevisiae* carrying *Pm*VRP15 gene was inoculated in an aerated 50-ml tube containing 10-ml URA medium 2.0 g/l of yeast synthetic drop-out medium without uracil and 6.7 g/l of yeast nitrogen base without amino acids) with 2% glucose and incubated overnight in an orbital shaker at 280 rpm at 30 ℃. The overnight culture was diluted to an $OD_{600}$ of 0.12 into a fresh 50-ml aerated tube, containing 10 ml-URA medium with 0.1% glucose. The cultures was incubated at 30 ℃ with 280 rpm shaking until an $OD_{600}$ reached 0.6. Expression of r*Pm*VRP15 was induced by addition of a final concentration of 2% (w/v) galactose. After 22 h, cells were harvested by centrifugation at 3,000 xg for 5 min and resuspended in YSB buffer (50 mM Tris–HCl pH 7.6, 5 mM EDTA, 10% glycerol and 1X complete protease inhibitor cocktail tablets). Cells were then disrupted by glass beads using a mixer-mill disruptor, set at 30 Hz for 10 min. Supernatant (soluble proteins) and pellet (inclusion body proteins) were separated by centrifugation at 8,000 xg for 20 min. Expression of r*Pm*VRP15 in soluble and inclusion body fractions was analyzed by 15% SDS-PAGE.

**3.7 Expression of recombinant *Pm*VRP15 in *Escherichia coli* expression system and protein purification**

**3.7.1 Cloning of full-length and truncated *Pm*VRP15 gene into pGEX4T-3 vector**

Full-length and truncated *Pm*VRP15 genes were amplified by PCR using specific primers (Table 3). The PCR condition was 94 °C for 3 min, followed by 30 cycles of 94 °C for 30 sec, 57 °C for 30 sec and 72 °C for 30 sec, and a final extension at 72 °C for 5 min. PCR products were analyze by 1.5% agarose gel.

**Table 3** Specific primers used for cloning full-length and truncated *Pm*VRP15 into pGEX4T-3 vector

| Primer | Sequence (5´-3´) |
|---|---|
| Full-length of *Pm*VRP15-F | GCGGGCCGGATCCATGTTAACAGAGGACTTAGTAAACCTGGTGTAC |
| Full-length of *Pm*VRP15-R | CTCGAGGCGTTTATAGGAGGCGATTCT |
| N-terminal part of *Pm*VRP15-F (residue 1-112) | GCGGGCCGGATCCATGTTAACAGAGGACTTAGTAAACCTGGTGTAC |
| N-terminal part of *Pm*VRP15-R | GCGGCCGCTTATGTTGAGACGAATGGTATGGAAG |
| C-terminal part of *Pm*VRP15-F (residue 186-414) | GGATCCTATGCTAGGGGGAAGTTCAAAAGC |
| C-terminal part of *Pm*VRP15-R | CTCGAGGCGTTTATAGGAGGCGATTCT |

*Pm*VRP15 fragments were ligated into pGEX4T-3 using *Bam*H I and *Not* I cloning sites; and the recombinant plasmids were transformed into *E. coli* TOP10 competent cells by heat shock method. The sequences of full-length and truncated *Pm*VRP15 genes were verified (Macrogen INC., South Korea).

### 3.7.2 Expression of full-length and truncated *Pm*VRP15 gene in pGEX4T-3

The *Pm*VRP15-recombinant pGEX4T-3 was transformed into *E. coli* C41 (DE3), C43 (DE3) or BL21-CodonPlus® (DE3) competent cells by heat shock method and transformants were grown on LB agar containing 100 µg/ml ampicillin at 37 °C overnight. A single colony of transformed *E. coli* was grown in LB medium containing 100 µg/ml ampicillin at 37 °C overnight with agitation at 250 rpm. The overnight culture was diluted 1:100 in fresh LB medium supplemented with 100 µg/ml ampicillin and grown until an $OD_{600}$ of the cultures reached 0.6. Protein expression was induced by addition of IPTG to final concentration of 1 mM. The cells were harvested at 1, 2, 3, 4 and 16 hour after IPTG induction by centrifugation at 8,000 x g for 10 min at 4 °C. Cells were then lysed by sonication for 10 rounds at 35% amplitude, pulse on 2 sec, pulse off 3 sec for 40 sec/round. Soluble and inclusion body protein fractions were separated by centrifugation at 12,000 rpm for 20 min at 4 °C. Expression of r*Pm*VRP15 was analyzed by 15% SDS-PAGE and Western blot.

### 3.7.3 Expression of full-length *Pm*VRP15 gene in pET22b(+)

The *Pm*VRP15-recombinant pET22b(+) was transformed into *E. coli* C43 (DE3) competent cells by heat shock method and transformants were grown on LB agar containing 100 µg/ml ampicillin at 37 °C overnight. A single colony of transformed *E. coli* C43 (DE3) carrying *Pm*VRP15 recombinant plasmid was grown in LB medium containing 100 µg/ml ampicillin at 37 °C overnight with agitation at 250 rpm. The overnight culture was diluted 1:100 in fresh LB medium supplemented with 100 µg/ml ampicillin and grown until an $OD_{600}$ of the cultures reached 0.6. Protein expression was induced by addition of IPTG to final concentration of 1 mM. The cells were harvested at 0, 1, 2, 3, 4, 5 and 6 hour post-induction by centrifugation at 8,000 xg for 10 min at 4 °C. The overexpression of recombinant *Pm*VRP15 (r*Pm*VRP15) was analyzed by SDS-PAGE and Western blotting.

### 3.7.4 Preparation of the r*Pm*VRP15

The *Pm*VRP15-recombinant pET22b(+) *E. coli* was grown in LB medium containing 100 µg/ml ampicillin at 37 °C overnight with agitation at 250 rpm. The culture was diluted 1:100 in fresh LB medium supplemented with 100 µg/ml ampicillin and grown until an $OD_{600}$ of the cultures reached

0.6. Cells were harvested at 1 h post-induction by centrifugation at 8,000 xg for 10 min at 4 °C and resuspended in 50 mM Tris-HCl buffer, pH 7.0 containing complete Protease inhibitor cocktail tablets (Roche). Cells were disrupted by sonication and the supernatant was collected by centrifugation at 8,000 xg, 4 °C for 20 min. Membrane fraction was obtained by centrifugation at 100,000 xg, 4 °C for 1 h and homogenized in 50 mM Tris-HCl buffer, pH 7.

**3.7.5 Purification of r*Pm*VRP15 by Nikel-nitrilotriacetic acid (Ni-NTA) Sepharose™ 6 Fast Flow**

Membrane-bound proteins were solubilized in solubilizing buffer (50 mM Tris-HCl, pH 7, 20 mM Imidazole, 300 mM NaCl, 20% glycerol and 1% n-decyl-ß-d-maltopyranoside, DM) at 4 °C overnight. Recombinant *Pm*VRP15 was purified using Ni-NTA Sepharose™ 6 Fast Flow (GE Healthcare). Crude proteins were incubated with Ni-NTA Sepharose™ 6 FF bead in binding buffer (50 mM Tris-HCl, pH 7, 20 mM Imidazole, 10% glycerol and 0.1% DM) and then, non-specific proteins were removed by wash buffer (50 mM Tris-HCl, pH 7, 50 mM Imidazole, 5% glycerol and 0.1% DM). The r*Pm*VRP15 protein was eluted with elution buffer (50 mM Tris-HCl, pH 7, 300 mM Imidazole, 5% glycerol and 0.1% DM). The purity of r*Pm*VRP15 was analyzed by 15% SDS-PAGE.

The partial purified r*Pm*VRP15 protein was applied onto HiTrap DEAE Fast Flow (GE Healthcare), equilibrated in binding buffer (20 mM Tris-HCl, pH 7, 20 mM NaCl, 10% glycerol and 0.1% DM). Non-specific proteins were removed by wash buffer (20 mM Tris-HCl, pH 7, 20 mM NaCl, 5% glycerol and 0.1% DM). The r*Pm*VRP15 protein was eluted with elution buffer (20 mM Tris-HCl, pH 7, 150 mM NaCl, 5% glycerol and 0.1% DM). The purified r*Pm*VRP15 was analyzed by 15% SDS-PAGE and Western blotting; and protein concentration was determined by Pierce® BCA Protein Assay Kit (Thermo scientific).

**3.8 Molecular characterization of r*Pm*VRP15**

**3.8.1. MALDI-TOF Mass spectrometry (MALDI-TOF MS)**

To determine the molecular weights of r*Pm*VRP15, purified r*Pm*VRP15 was sent to Mahidol University for MALDI-TOF MS analysis.

**3.8.2 Circular Dichroism (CD) spectroscopy**

Secondary structure of purified r*Pm*VRP15 was analyzed by circular dichroism (CD) spectroscopy using JASCO J-715 CD Spectropolarimeter with temperature controller and a 1 mm optical cuvette. The (+)-10-camphorsulfonic acid (CSA) was used as calibration standard before measuring CD spectrum. Spectra were recorded between 180-320 nm using a bandwidth of 2 nm and a response time of 2 sec with 50 mm/min scanning speed. Each spectrum was the average of three scans and background was subtracted with the spectrum of 10 mM Phosphate buffer pH 7.0 (blank). The CD spectra of purified r*Pm*VRP15 (0.42 mg/ml) were analyzed using K2D3 (Louis-Jeune et al, 2011).

**3.8.3 Size-exclusion chromatography**

Size-exclusion chromatography (SEC) was performed to analyze protein aggregates. Superdex 200 column (GE Healthcare) was equilibrated with 10 mM Tris-HCl, pH 7.5 and 150 mM NaCl buffer with or without 0.087% DM. Purified r*Pm*VRP15 was applied onto column in buffers with and without 0.087% DM. A protein standard mix (Bio-RAD) of thyroglobin (670 kDa), $\gamma$-globulin (158 kDa), ovalbumin (44 kDa), myoglobin (17 kDa) and vitamin B12 (1,350 Da) was used in this experiment.

**3.8.4 Analytical ultracentrifugation**

Size distribution of r*Pm*VRP15 was analyzed by analytical ultracentrifugation (AUC). Sedimentation velocity experiments were performed on an Optima XL-A analytical ultracentrifuge (Beckman Instruments) with an An-60 Ti rotor. Purified *Pm*VRP15 of 60 $\mu$M was dissolved in 10 mM Tris-HCl, pH 7.5, 100 mM NaCl and 0.03% n-dodecyl $\beta$-D maltoside (DDM). The sample and reference

buffer were injected into each side of a double-sector centerpiece and centrifuged at 20,000 rpm at 20 °C for 16.5 h. The spectrum was monitored continuously using a time interval of 600 s per scan. The dataset from these multiple scans at 280 nm at different time intervals were then fitted to a continuous c(s) distribution model using the SEDFIT program (Brown & Schuck, 2006; Schuck, 2000). The partial-specific volume of *Pm*VRP15 was calculated to be 0.73 ml/g, based on the solvent density of 1.035 g/ml and the viscosity of 1.83 cP

**3.9 Crystallization of r*Pm*VRP15**

In this study, Crystal Screen 1, 2™, PEG/Ion 1, 2 ™, Index™, MembFac™ (Hampton Research), JCSG Core I, II, III, IV Suits, PACT Suits (Qiagen) were used. Drops of protein and reservoir solution were set up at the ratio of 1:1 in 96-well crystallization plate using sitting drop vapor diffusion method. Crystallization plates were incubated at 18 °C and observed weekly thereafter for three months. Crystals obtained from 96-well plate were cryo-protected and frozen in liquid nitrogen before testing the diffraction of a crystal at BL13B1 of the National Synchrotron Radiation Research Center (NSRRC, Taiwan). Recombinant *Pm*VRP15 was also treated with alkylating reagent and dimethylamine borane complex in order to modify lysine residues, prior to crystallization trials.

**4. Results**

**4.1 Expression of *Pm*VRP15 in unchallenged- and WSSV-challenged *P. monodon* primary hemocyte cultures**

*Pm*VRP15 expression in unchallenged and WSSV-challenged *P. monodon* primary hemocyte cultures was examined by RT-PCR. Clearly, *Pm*VRP15 transcripts were apparently increased after 12 h post-WSSV infection onwards (Figure 1).

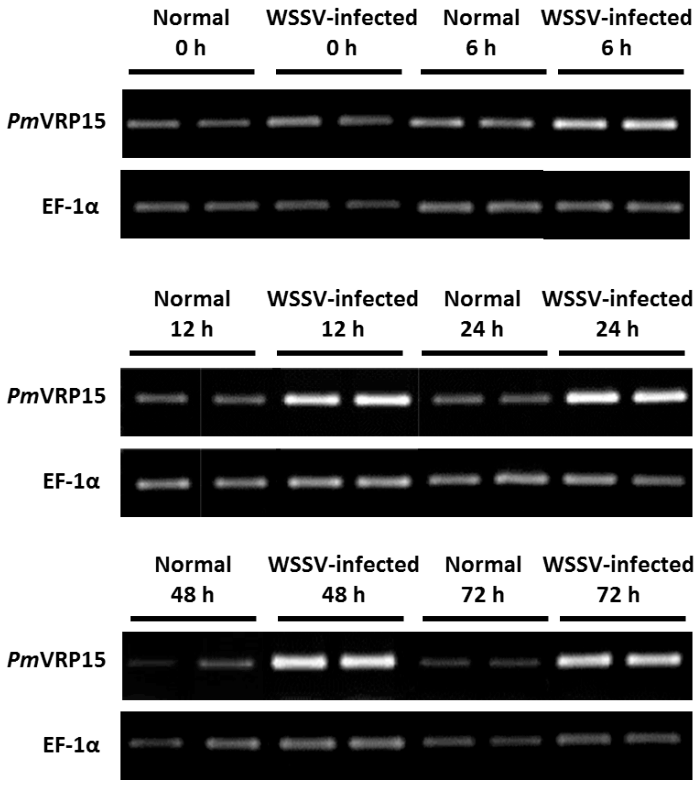


**Figure 1** *Pm*VRP15 mRNA levels in response to WSSV infection. Relative expression ratios of *Pm*VRP15 transcript levels was determined in WSSV-infected *P. monodon* hemocytes by RT-PCR, compared to control (non-infected) shrimp and standardized against elongation factor-1 alpha (EF-1$\alpha$) as an internal reference, at 0, 6, 12, 24, 48 and 72 h post-WSSV infection.

Real-time RT-PCR confirmed that *Pm*VRP15 mRNA expression was up-regulated by 2.6, 3.6, 6.7 and 4.1 fold at 12, 24, 48 and 72 h post-WSSV infection, respectively (Figure 2). These results indicated that *Pm*VRP15 was highly expressed in *P. monodon* primary hemocyte cultures in response to WSSV infection.

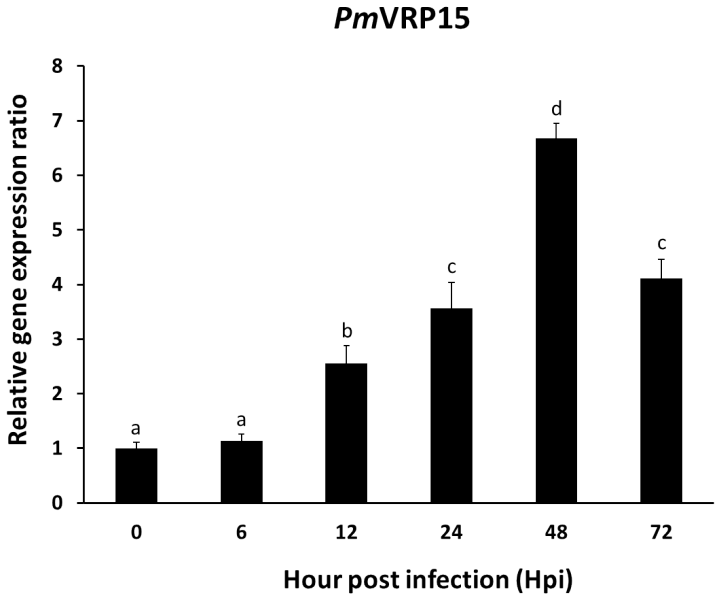


**Figure 2** Up-regulation of *Pm*VRP15 mRNA in response to WSSV infection. Relative expression ratios of *Pm*VRP15 transcript levels was determined in WSSV-infected *P. monodon* hemocytes by real time RT-PCR, compared to control (non-infected) shrimp and standardized against elongation factor-1 alpha (EF-1 alpha) as the internal reference, at 0, 6, 12, 24, 48 and 72 h post-WSSV infection. The statistical significance of the data was evaluated using one-way ANOVA followed by post hoc test (Duncan's new multiple range test). Data differences were considered significant at $P < 0.01$.

**4.2 *In vitro* double strand RNA-mediated knockdown of *Pm*VRP15 gene expression resulted in reduction of WSSV propagation**

In this study, RNA interference (RNAi) technique was used to knockdown *Pm*VRP15 transcript in order to investigate the function of *Pm*VRP15. Primary hemocyte cell cultures were treated with either *Pm*VRP15 dsRNA or GFP dsRNA (control) prior to WSSV infection. After 24 h, expressions of *Pm*VRP15, VP28 and EF-1$\alpha$ (an internal reference) were analyzed by RT-PCR (Figure 3). This result showed that knockdown of *Pm*VRP15 gene resulted in the reduction of VP28 transcripts.

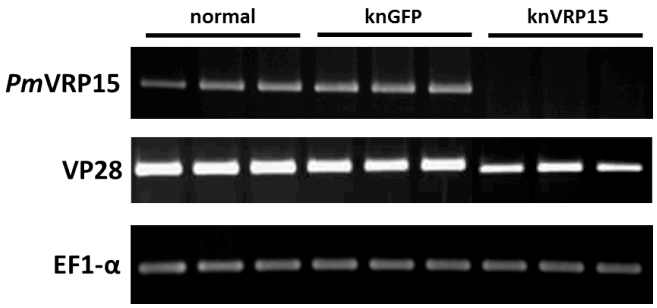


**Figure 3** Silencing of *Pm*VRP15 expression in WSSV-infected *P. monodon* hemocytes resulted in the reduction of VP28 gene expression. RT-PCR analysis of VP28 and *Pm*VRP15 gene of hemocytes shrimp primary cell culture at 24 hour post WSSV injection.

Quantitative Real-time RT-PCR confirmed that VP28 expression level decreased by approximately 4.17 fold (84%) at 24 h post WSSV-infection compared to that of the control (Figure 4). This result suggested that *Pm*VRP15 is important for WSSV propagation in *P. monodon* hemocytes.

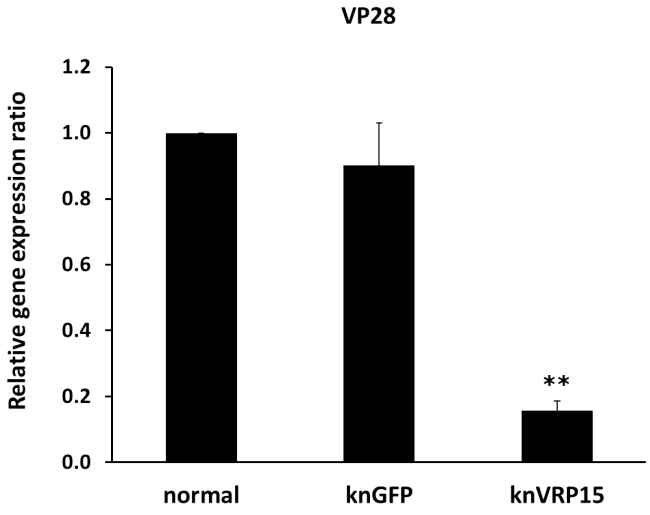


**Figure 4** Silencing of VRP15 mRNA in response to WSSV propagation. Relative expression ratios of VP28 transcription level was determined in WSSV-infected *P. monodon* hemocytes by real time RT-PCR, compared to control (normal WSSV-infected shrimp hemocytes) and standardized against elongation factor-1 alpha (EF-1 alpha) as an internal reference, at 24 h post-WSSV infection. The data represent the mean ($\pm$ 1 SD) relative expression of VP28, derived from three independent experiments. Means with an asterisk are significantly different ($P < 0.01$).

**4.3 Immunolocalization of *Pm*VRP15 and VP28 in normal and *Pm*VRP15-knockdown hemocytes infected by WSSV**

*Pm*VRP15 and VP28 in *Pm*VRP15-silenced and GFP-silenced hemocytes at 48 h post-WSSV infection was examined by confocal laser scanning microscopy using the antibodies specific to *Pm*VRP15 and VP28 coupled with different fluorescene-conjugated secondary antibodies. *Pm*VRP15 (in green color) was observed in all three types of hemocytes, including granular cells (GC) semi-granular cells (SGC) and hyaline cells (HC), at 48 h post-WSSV infection (Figure 5). *Pm*VRP15 protein was located at the edge of nucleus, or possible at the nuclear membrane of the cell. Hemocytes of kn*Pm*VRP15 showed lower amounts VP28 than those of knGFP cells. This indicated that knockdown of *Pm*VRP15 reduced WSSV propagation.

It is worth noting that the green fluorescent signal of *Pm*VRP15 was still observed in *Pm*VRP15-silenced hemocytes; however, the intensity of the signal was lower than that observed in the control (GFP-silenced hemocytes). This indicated *Pm*VRP15 was not completely silenced at 48 hpi, the time point at which *Pm*VRP15 was expressed at the highest level (Figure 2).

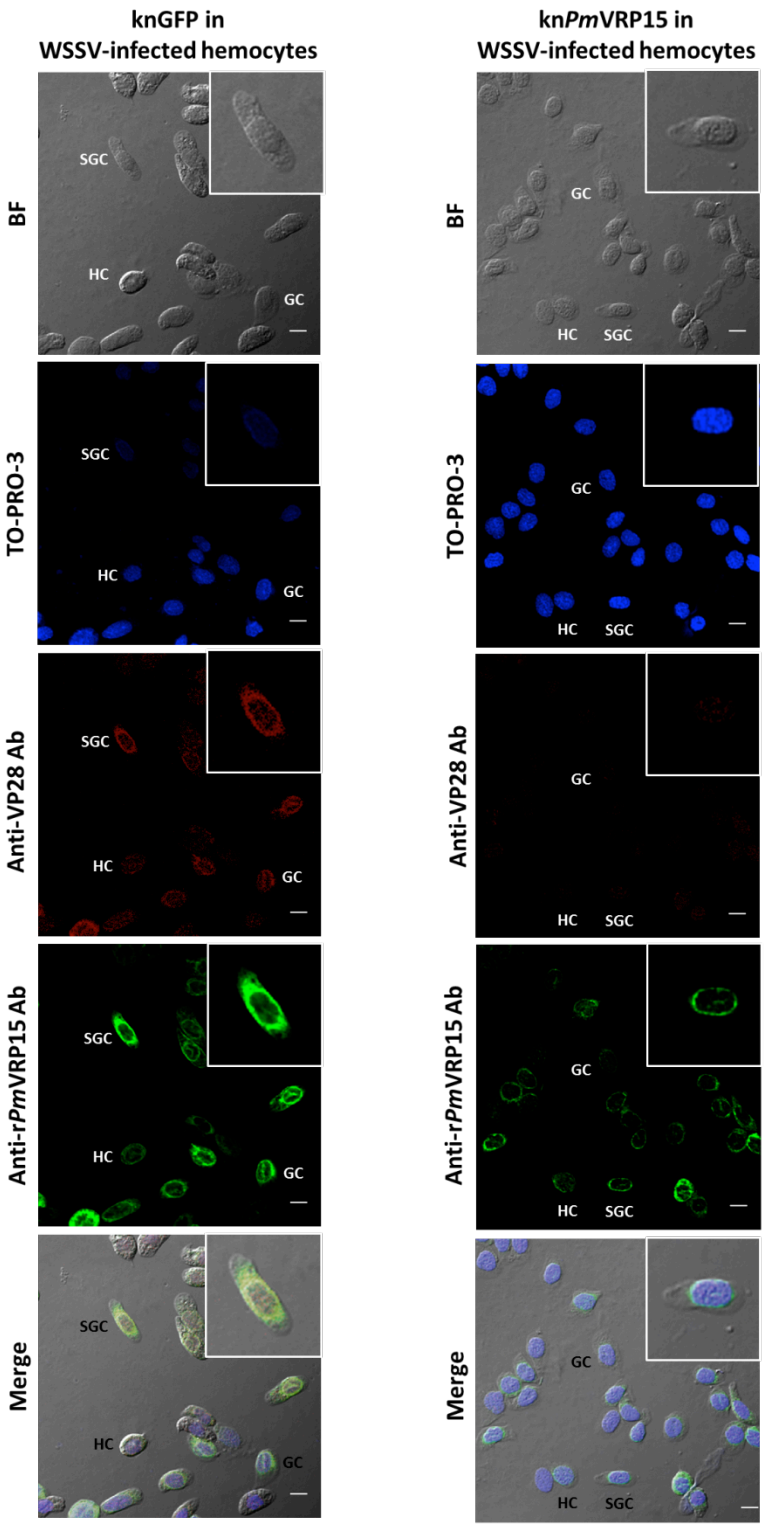


**Figure 5** Immunolocalization of *Pm*VRP15 and VP28 in *Pm*VRP15-silenced and GFP-silenced hemocytes at 48 h post-WSSV infection. Rabbit anti-r*Pm*VRP14 and mouse anti-VP28 primary antibodies were detected with corresponding Alexa488 and Alexa568 secondary antibodies, showing

*Pm*VRP15 (green color) and VP28 (red color), respectively. TO-PRO-3 iodide was used for nuclei staining and color was adjusted to blue. The GC, SGC and HC are granular, semigranular and hyaline cells, respectively. BFs are bright field images. The scale bar corresponds to 5 μm. Images are representative of 3 fields of view per sample.

**4.4 Protein localization of *Pm*VRP15 by subcellular protein fractionation**

Cytoplasmic, membrane, soluble nuclear, chromatin-bound and cytoskeletal fractions were extracted from WSSV-infected hemocyte cultures using subcellular fractionation kit. Figure 6 showed that *Pm*VRP15 protein was found in soluble nuclear, and chromatin-bound fractions. This indicated that *Pm*VRP15 is a nuclear localized protein.

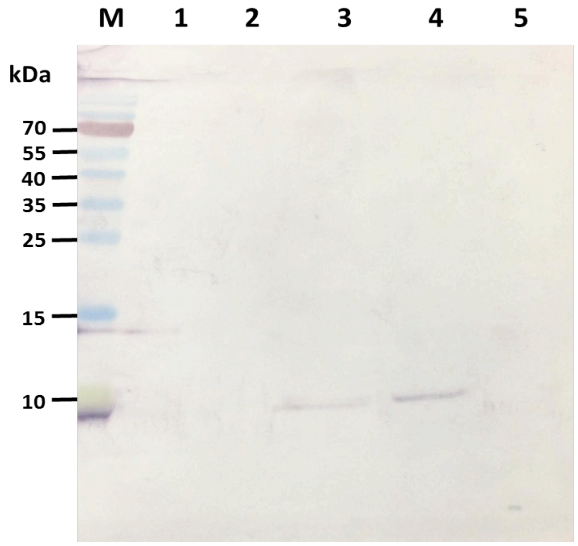


**Figure 6** Western blotting analysis of the *Pm*VRP15 protein in WSSV-infected hemocytes. Lane M is a protein marker. Lane 1-5 are cytoplasmic, membrane, soluble nuclear, chromatin-bound and cytoskeletal fraction, respectively.

**4.5 Roles of *Pm*VRP15 in nuclear import and export of WSSV**

The silencing of *Pm*VRP15 in WSSV-infected hemocytes was performed in order to identify a possible role of *Pm*VRP15 in nuclear entry or exit of WSSV. First, silencing of *Pm*VRP15 by VRP15 dsRNA treatment was confirmed by Western blotting using β-actin as an internal control. β-actin (43 kDa) was found in both GFP dsRNA- and VRP15 dsRNA treated hemocyte lysates of similar amount, while *Pm*VRP15 (15 kDa) was found only in GFP dsRNA treated hemocytes, but not *Pm*VRP15 VRP15 dsRNA treated cells (Figure 7). This indicated that VRP15 dsRNA injection successfully suppressed *Pm*VRP15 expression.

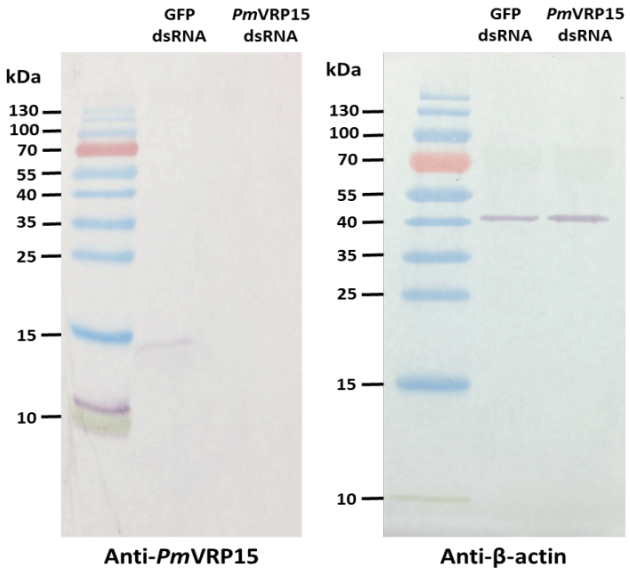


**Figure 7** RNAi-mediated suppression of *Pm*VRP15 (VRP15 dsRNA) resulted in a reduction of protein level. GFP dsRNA was used as a control.

Next, cytoplasmic and nuclear fractions were extracted from WSSV-infected GFP- or *Pm*VRP15 knockdown hemocyte cells and subjected to quantification of WSSV copy number in each fraction. Western blotting using Nuclear Pore Complex (NPC) antibody as primary antibody was performed in order to confirm there was no cross-contamination between cytoplasmic and nuclear fractions (Figure 8). Apparently, NPC was detected in nuclear fractions of *Pm*VRP15-silenced and GFP-silenced hemocytes only.

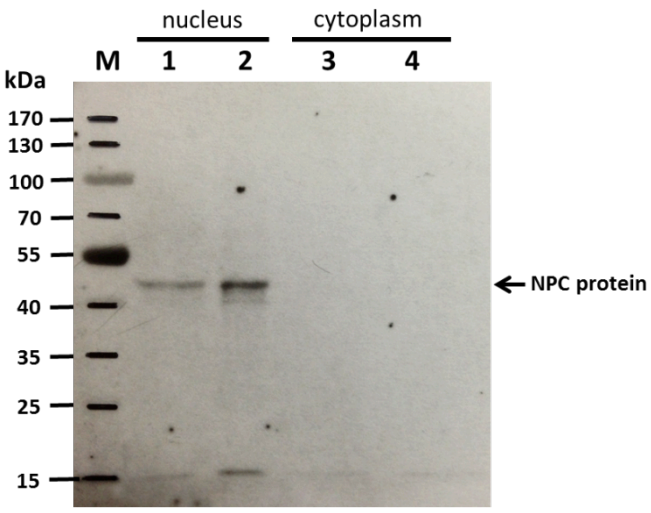


**Figure 8** Western blot analysis of cytoplasmic and nuclear fractions of WSSV-infected *Pm*VRP15-silenced and GFP-silenced hemocytes using Pierce® Fast Western Blot Kit, SuperSignal® West Femto kit. NPC protein was detected using anti-NPC (Abcam) as primary antibody and Fast Western Mouse Optimized HRP Reagent, Femto as secondary antibody, respectively. X-ray film was developed to observed the signals. Lane 1 is nuclear fractions of WSSV-infected GFP-silenced. Lane 2 is nuclear fractions of WSSV-infected *Pm*VRP15-silenced. Lane 3 is cytoplasmic fractions of WSSV-infected GFP-silenced. Lane 4 is cytoplasmic fractions of WSSV-infected GFP-silenced.

Table 4 shows the ratio of WSSV DNA in nuclear to cytoplasmic fractions of *Pm*VRP15 dsRNA and GFP dsRNA samples. The experiment was carried out in triplicate and EF-1$\alpha$ was used for normalization of WSSV DNA quantification. The result showed that the ratio of DNA virus (WSSV) in nucleus to cytoplasmic fraction of *Pm*VRP15-silenced was lower than that of control (GFP-silenced hemocytes) by 9.28 fold. This suggested that *Pm*VRP15 plays a role in nuclear entry of WSSV.

**Table 4** The ratio of WSSV copy number of PmVRP15 silencing in nucleus/cytoplasm compare to control (GFP-silenced hemocytes)

| Sample | WSSV in Cytoplasm | WSSV in Nucleus | Average (Nucleus) | Ratio of WSSV in Nucleus/Cytoplasm | Means | Fold |
|---|---|---|---|---|---|---|
| knGFP | 3.83E-03 | 3.92E-02 | 3.82E-02 | 9.97E+00 | 1.11E+01 | **9.28E+00** |
| | 2.95E-03 | 3.49E-02 | | 1.29E+01 | | |
| | 3.64E-03 | 4.04E-02 | | 1.05E+01 | | |
| knVRP15 | 1.60E-02 | 2.72E-02 | 1.88E-02 | 1.17E+00 | 1.20E+00 | |
| | 1.47E-02 | 1.28E-02 | | 1.27E+00 | | |
| | 1.63E-02 | 1.62E-02 | | 1.15E+00 | | |

### 4.6 Expression of r*Pm*VRP15 protein in *S. cerevisiae*

*Pm*VRP15 gene was successfully amplified and subcloned into pDDGFP-2 vector (data not shown). Expression of r*Pm*VRP15 in *S. cerevisiae* (FGY217) was induced by 2% (w/v) galactose at 30 ℃ for 22 h. Soluble and inclusion body protein fractions were analyzed by 15% SDS-PAGE (Figure 9). Apparently, no major protein band of 15 kDa was observed in any fractions of the induced sample. This indicated that r*Pm*VRP15 was not expressed in this condition.

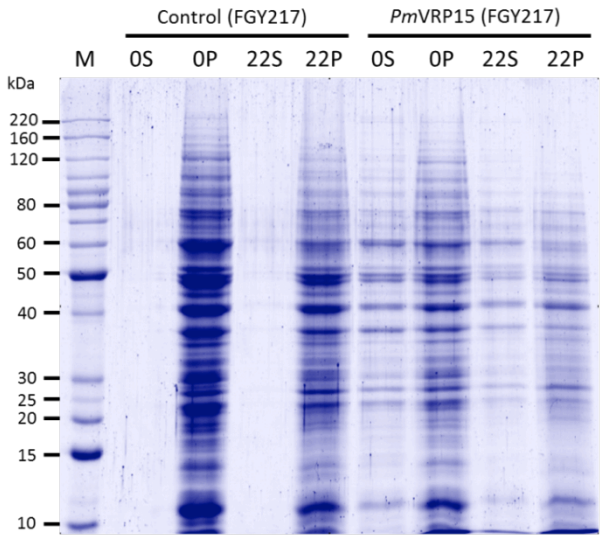


**Figure 9** Protein expression of r*Pm*VRP15 in *S.cerevisiae* (FGY217). 0S; soluble protein at 0 h post-galactose induction, 0P; pellet or inclusion bodies protein at 0 h post-galactose induction, 22S; soluble protein at 22 h post-galactose induction, 22P; pellet or inclusion bodies protein at 22 h post-galactose induction.

**4.7 Cloning and expression of full-length and truncated *Pm*VRP15 gene in pGEX4T-3**

Full-length and truncated *Pm*VRP15 genes were amplified by PCR from cDNA using specific primers as shown in Table 3. PCR products of full-length and truncated *Pm*VRP15 genes were analyzed by 1.5% (w/v) agarose gel electrophoresis (Figure 10). Estimated sizes of PCR products of full-length, N-terminal truncated and C-terminal truncated of *Pm*VRP15 are 414 bp, 112 bp and 229 bp, respectively.

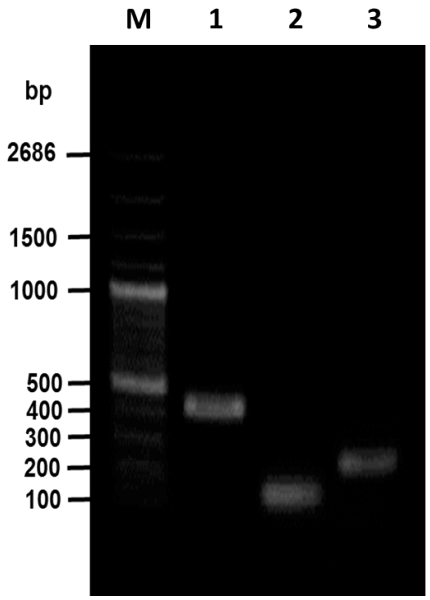


**Figure 10** PCR products of full-length, N-terminal truncated and C-terminal truncated of *Pm*VRP15. Lane 1 is a full-length *Pm*VRP15 gene. Lane 2 is an N-terminal truncated *Pm*VRP15 gene. Lane 3 is a C-terminal truncated *Pm*VRP15 gene.

In Figure 11, full-length *Pm*VRP15-GST fusion protein was expressed mostly in inclusion bodies in *E. coli* C41 (DE3) and C43 (DE3). Similarly, N-terminal truncated *Pm*VRP15 was expressed in *E. coli* C41 (DE3) and C43 (DE3) in inclusion bodies (Figure 12). This indicated that removal of predicted transmembrane helix of *Pm*VRP15 did not increase protein solubility. C-terminal truncated *Pm*VRP15 was expressed in *E. coli* BL21-CodonPlus® (DE3) at 37°C and 16°C. C-terminal truncated *Pm*VRP15-GST fusion protein was expressed mostly in inclusion bodies at both temperatures (Figure 13). It is likely that expression of C-terminal truncated *Pm*VRP15-GST fusion protein at lower temperature did not improve protein solubility.

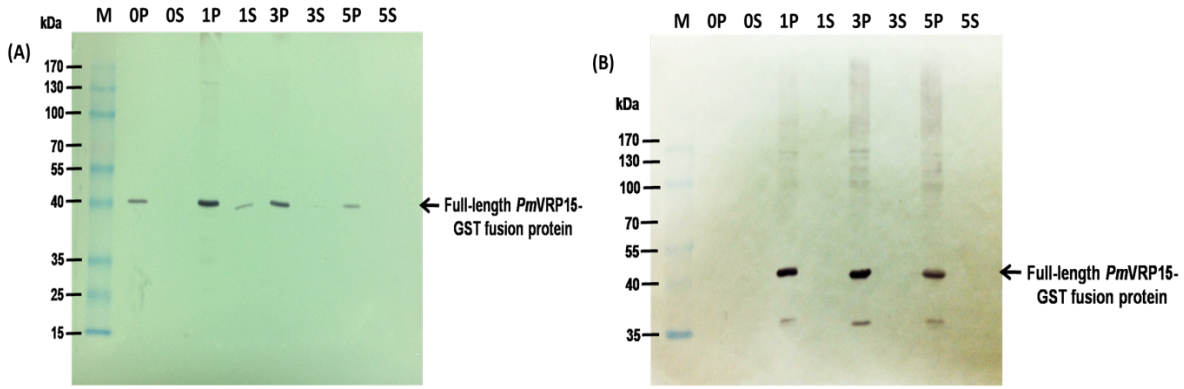


**Figure 11** Western blotting analysis of full-length *Pm*VRP15-recombinant pGEX4T-3. The recombinant protein was expressed in *E. coli* C41 (DE3) (A) and *E. coli* C43 (DE3) (B) at 0 h, 1 h, 3 h and 5 h after induction by IPTG at 37°C (S; soluble fraction, P; pellet or inclusion bodies protein fraction). An arrow indicates full-length *Pm*VRP15-GST fusion protein.

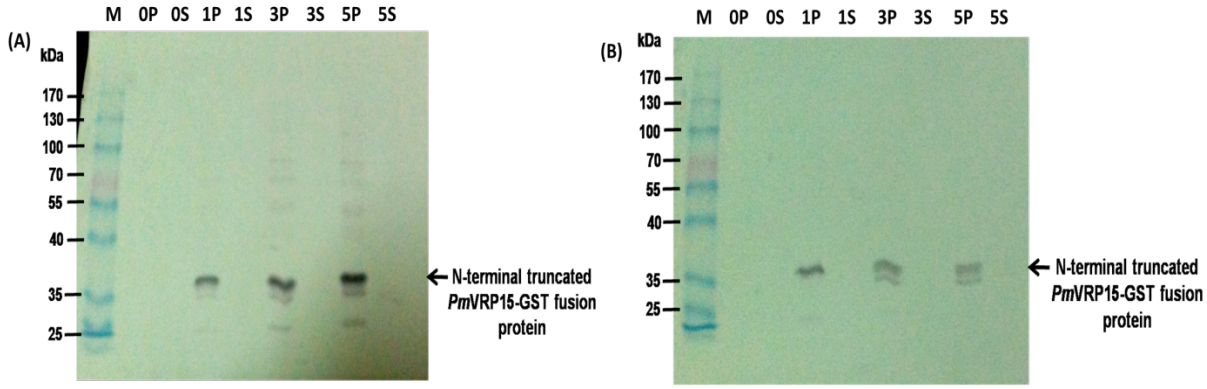


**Figure 12** Western blotting analysis of N-terminal truncated *Pm*VRP15-recombinant pGEX4T-3. The recombinant protein was expressed in *E. coli* C41 (DE3) (A) and *E. coli* C43 (DE3) (B) at 0 h, 1 h , 3 h and 5 h after induction by IPTG at 37°C (S; soluble fraction, P; pellet or inclusion bodies protein fraction). An arrow indicates N-terminal truncated *Pm*VRP15-GST fusion protein.

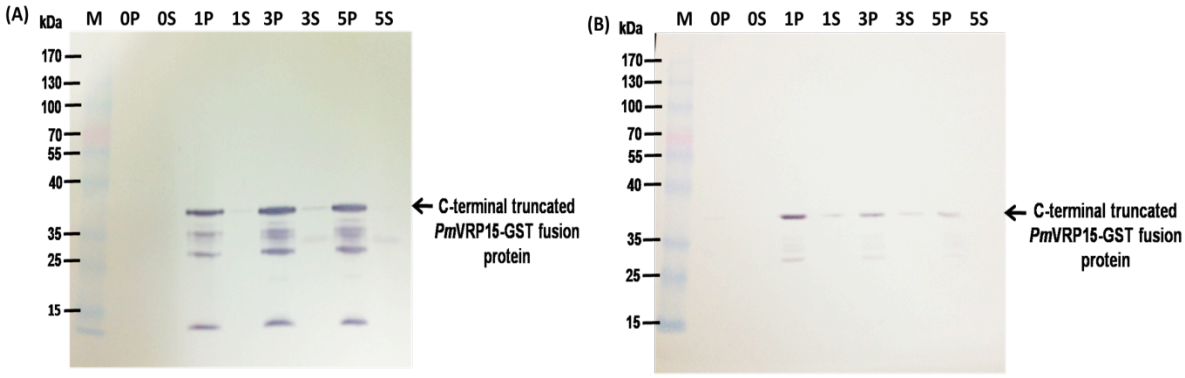


**Figure 13** Western blotting analysis of C-terminal truncated *Pm*VRP15-recombinant pGEX4T-3. The recombinant protein was expressed in *E. coli* BL21-CodonPlus® (DE3) at 37 °C (A) and 16 °C (B) at 0 h, 1 h, 3 h and 5 h after induction by IPTG (S; soluble fraction, P; pellet or inclusion bodies protein fraction). An arrow indicates C-terminal truncated *Pm*VRP15-GST fusion protein.

### 4.8 Expression of full-length *Pm*VRP15 gene in pET22b(+)

Expression of full-length *Pm*VRP15 gene in pET22b(+) was carried out in the *E. coli* C43 (DE3) at 37 °C. The result showed that r*Pm*VRP15 was expressed at 1-3 h post-IPTG induction and expressed in the highest level at 2 h post-IPTG induction (Figure 14). Noticeably, no r*Pm*VRP15 band was observed on Western blot membrane after 3 h post-IPTG induction. This may indicate that r*Pm*VRP15 was a toxic protein or it was unstable.

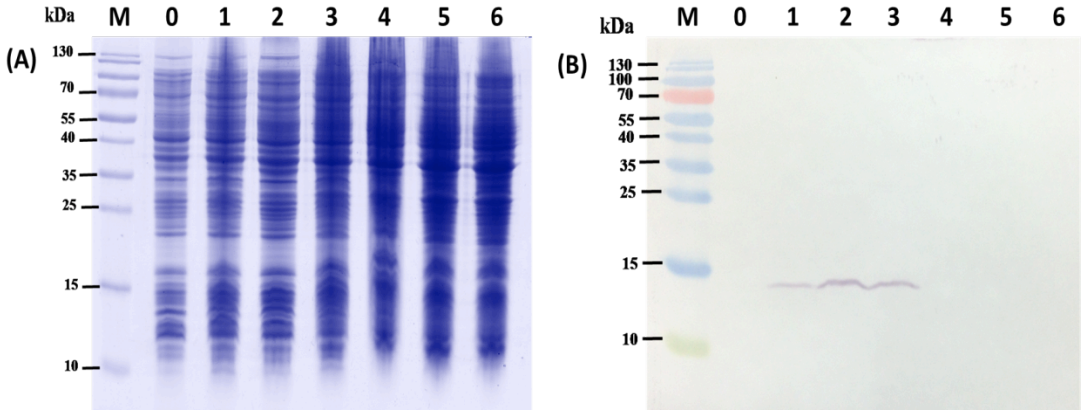


**Figure 14** Expression of r*Pm*VRP15 in *E. coli* C43 (DE3) analyzed by coomassie brilliant blue staining (A) and Western blotting (B). The r*Pm*VRP15 was expressed in *E. coli* C43 (DE3) and induced with 1 mM IPTG for 0, 1, 2, 3, 4, 5 and 6 hour. Lane M is the protein marker.

For 1 h induction, r*Pm*VRP15 was found in both soluble and inclusion body protein fractions (Figure 15). However, r*Pm*VRP15 was expressed only in inclusion bodies for 2 h and 3 h post IPTG-induction.

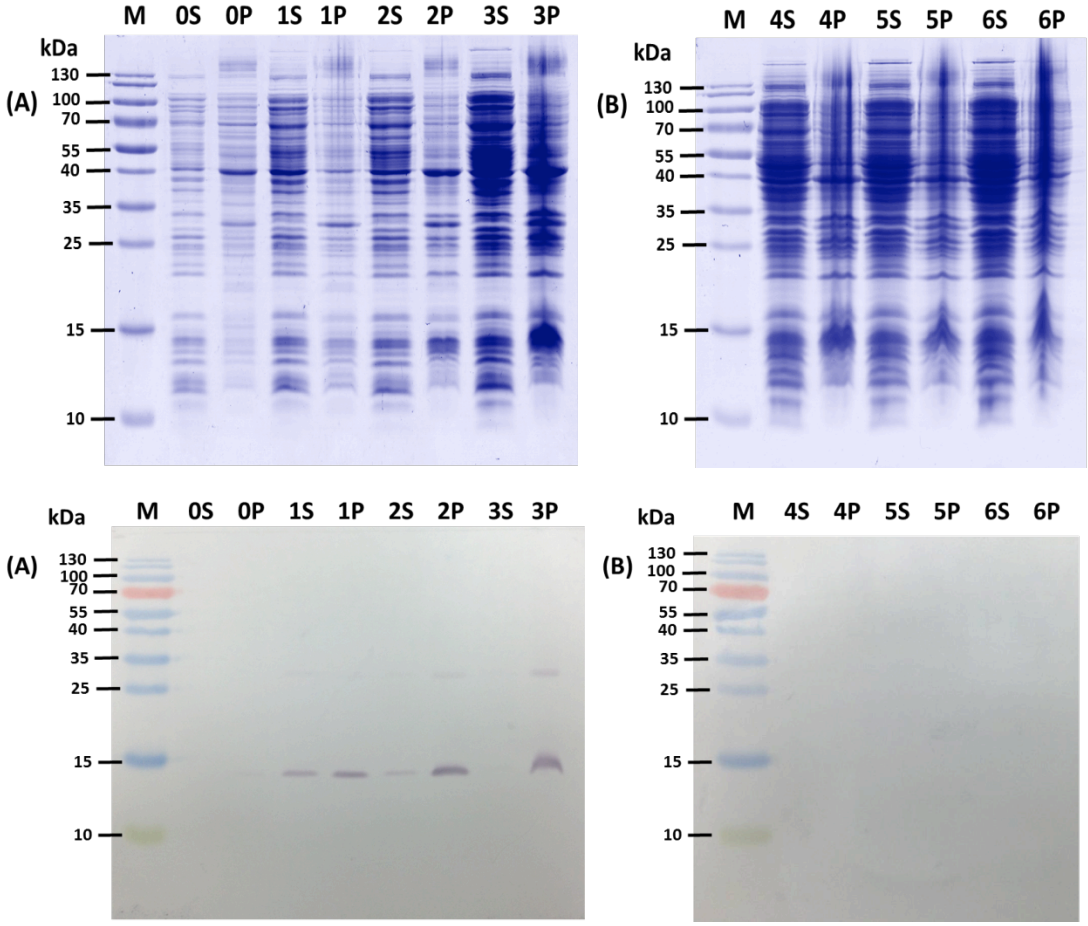


**Figure 15** Coomassie brilliant blue staining (upper panel) and Western blotting (lower panel) of r*Pm*VRP15 in *E. coli* C43 (DE3). (S; soluble fraction, P; pellet or inclusion bodies protein fraction).

### 4.9 Purification of r*Pm*VRP15

Recombinant *Pm*VRP15 was purified by Ni-NTA Sepharose™ 6 Fast Flow and HiTrap DEAE Fast Flow (GE Healthcare) as described in Research Methodology section. Purified r*Pm*VRP15 was analyzed by 15% SDS-PAGE and Western blotting (Figure 16). The protein band of 15 kDa was identified as r*Pm*VRP15 using anti-His antibody.

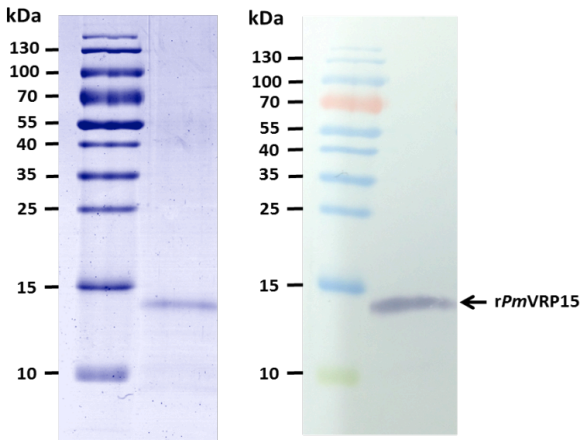


**Figure 16** 15% SDS-PAGE of purified r*Pm*VRP15 by coomassie brilliant blue staining (A) and Western blotting (B).

### 4.10 Molecular characterization of r*Pm*VRP15

#### 4.10.1 MALDI-TOF Mass spectrometry

MALDI-TOF MS analysis showed that the molecular mass of rPmVRP15 was 15,899.9 Da (Figure 17).

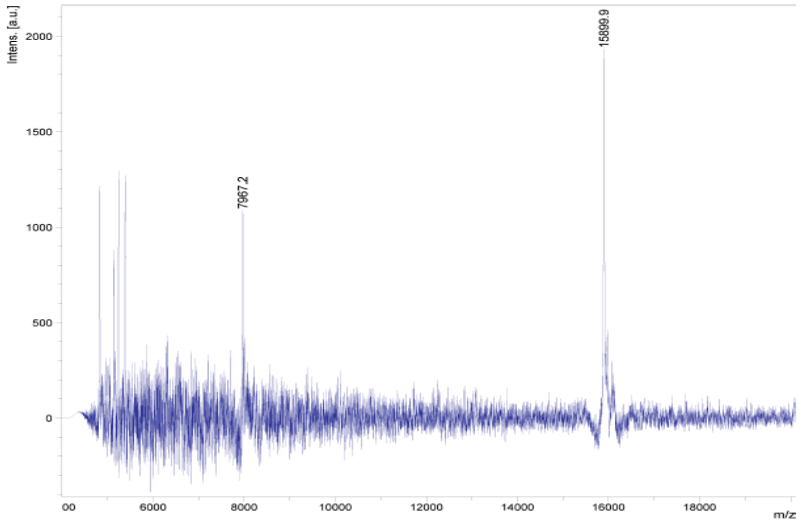


**Figure 17** MALDI-TOF MS analysis of r*Pm*VRP15.

### 4.10.2 Circular Dichroism (CD) spectroscopy

Figure 18 showed CD spectrum of r*Pm*VRP15. The amount of secondary structures ($\alpha$-helix and $\beta$-strand) of r*Pm*VRP15 was estimated by analyzing the CD spectrum using K2D3 software. The result showed that rPmVRP15 contained 48.45% $\alpha$-helix and 13.57% $\beta$-strand.

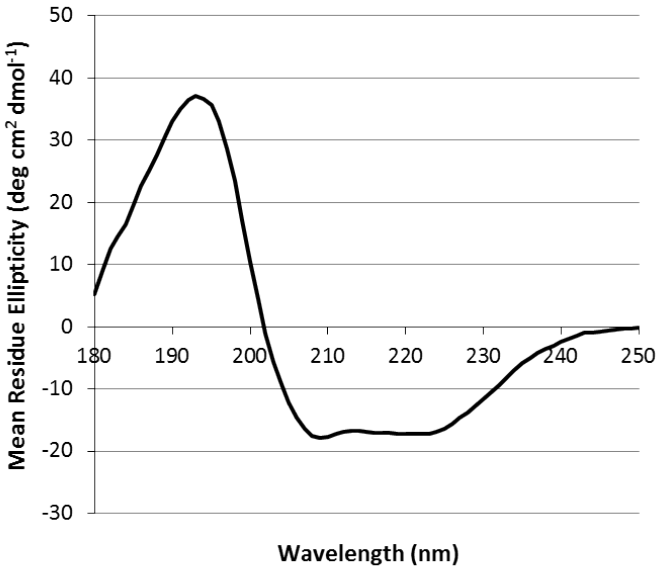


**Figure 18** CD spectrum of r*Pm*VRP15. The major secondary structure type of rPmVRP15 is $\alpha$-helix.

### 4.10.3 Size-exclusion chromatography (SEC)

Size-exclusion chromatography (SEC) was performed to monitor protein aggregation. Superdex 200 column (GE Healthcare) was equilibrated with 10 mM Tris-HCl, pH 7.5 and 150 mM NaCl buffer with or without 0.087% DM. A protein standard mix and purified r*Pm*VRP15 was then applied onto the column. Figure 19 showed that r*Pm*VRP15 was aggregated in equilibration buffer without DM as the protein came out in early fractions (left panel). In contrast, r*Pm*VRP15 seemed to be soluble in equilibration buffer with DM (right panel). This suggested that it is necessary to include detergent in buffer to maintain r*Pm*VRP15 solubility.

(A) Standard Proteins

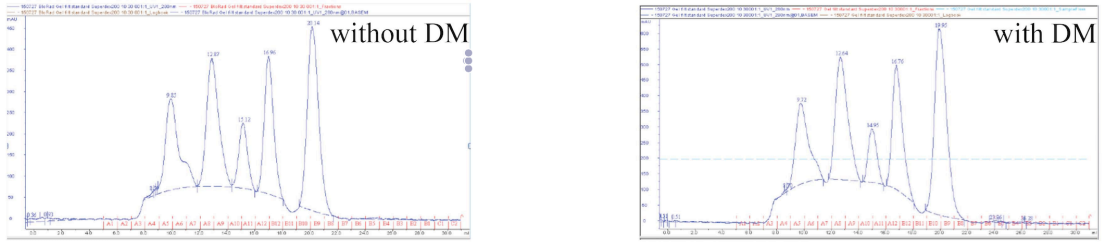


(B) r*Pm*VRP15

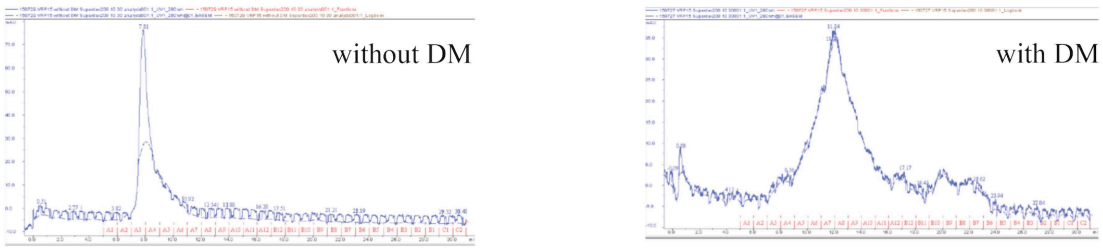


**Figure 19** SEC chromatograms of r*Pm*VRP15 analyzed using Superdex 200 column. A protein standard mix contains thyroglobin (670 kDa), γ-globulin (158 kDa), ovalbumin (44 kDa), myoglobin (17 kDa) and vitamin B12 (1,350 Da).

### 4.10.4 Analytical Ultracentrifugation (AUC)

Ultracentrifuge sedimentation-velocity analysis of purified *Pm*VRP15 (60 μM) in 10 mM Tris-HCl, pH 7.5, 100 mM NaCl and 0.03% n-dodecyl β-D maltoside (DDM) showed a major peak of 172 kDa (Figure 20). Assuming that molar mass of r*Pm*VRP15 bound to detergent was 39.5 kDa, a major peak of 172 kDa was corresponding to tetramer. This result indicated that *Pm*VRP15 at 60 μM could possibly form a tetramer.

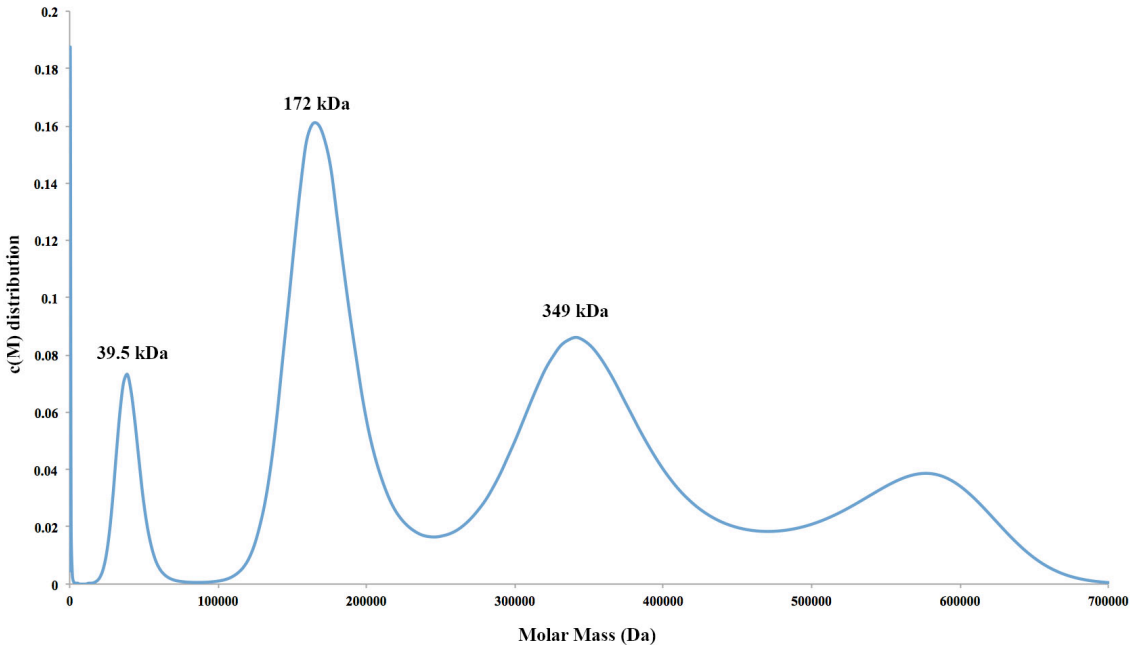


**Figure 20** Ultracentrifuge sedimentation-velocity analysis of r*Pm*VRP15. The molar mass distribution curve obtained from the experiment shows a major peak of 172 kDa.

### 4.11 Crystallization of r*Pm*VRP15

In this study, Crystal Screen 1, 2™, PEG/Ion 1, 2 ™, Index™, MembFac™ (Hampton Research), JCSG Core I, II, III, IV Suits, PACT Suits (Qiagen) were used to screen for crystallization conditions of r*Pm*VRP15. Some crystals appeared in 96-well crystallization plates and were tested for X-ray diffraction (Figure 21A). However, no well-diffracted protein crystal was found (Figure 21B).

Reductive methylation of free amino groups is an efficient method for improving/obtaining crystals. Generally, methylated proteins retain their biochemical function (Kobayashi et al, 1999; Rypniewski et al, 1993). In this work, r*Pm*VRP15 was treated with alkylating reagent and dimethylamine borane complex in order to modify lysine residues (Rayment, 1997). Then, methylated r*Pm*VRP15 was used for crystallization trials using Crystal Screen 1, 2™, Index™, and MembFac™ (Hampton Research). Unfortunately, no protein crystal was obtained.

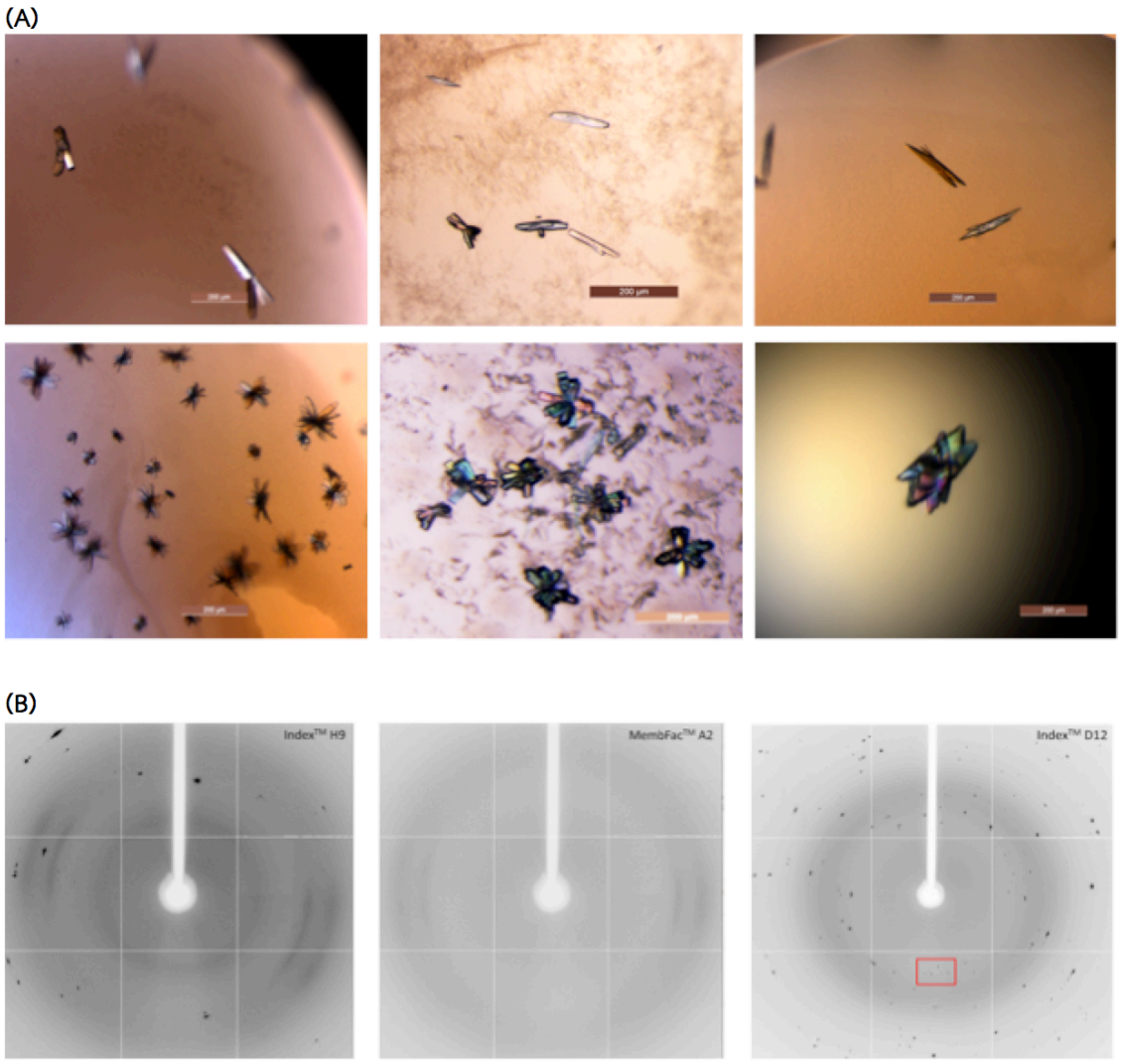


**Figure 21** Crystals appeared in 96-well plate (A) and their diffraction patterns (B)

## 5. Discussion

In primary hemocyte cultures, *Pm*VRP15 was up-regulated from 12 h after WSSV infection onwards (Figure 2). *Pm*VRP15 transcripts increased by about 2.6, 3.6, 6.7 and 4.1 fold at 12, 24, 48 and 72 h post-WSSV infection, respectively. The highest level of *Pm*VRP15 expression in primary hemocyte cell cultures was observed at 48 h after WSSV infection, which is in agreement with *In vivo* study (Vatanavicharn et al, 2014). Knockdown of *Pm*VRP15 *in vitro* prior to WSSV infection also caused a reduction of VP28 transcripts by 4.17 fold (Figure 4). This result suggested that *Pm*VRP15 is important for WSSV propagation in *P. monodon* hemocytes.

Confocal laser scanning microscopy revealed that *Pm*VRP15 protein was expressed in all three types of hemocytes, including granular (GC), semigranular (SGC) and hyaline cells (HC), at 48 h post WSSV infection (Figure 5). The expression of *Pm*VRP15 protein was located at the edge of nucleus, or possible at the nuclear membrane of the cell. Hemocytes of kn*Pm*VRP15 showed lower amounts VP28 than those of knGFP cells. This indicated that knockdown of *Pm*VRP15 reduced WSSV propagation.

Subcellular protein fractionation demonstrated that *Pm*VRP15 was found in soluble nucleus and chromatin-bound fractions (Figure 6). This implied that *Pm*VRP15 is a nuclear localized protein. Protein-structural analysis predicted that *Pm*VRP15 contained a transmembrane helix of 23 amino acids (TMHMM Server v. 2.0) (Krogh et al, 2001). Thus, this transmembrane helix may be important for nuclear membrane binding.

Viral envelopes are frequently structural components of the virus that mediate the crucial tasks of receptor recognition and membrane fusion. Fusion of viral envelope with the host's membrane allows the capsid and viral genome to enter host cells and initiate viral replication. Viruses that replicate in the nucleus of host cells transfer their genomes through the nuclear pore complex (NPC) into the nucleus. The strategies to target the NPC differ among viruses but invariably involve specific pathways of signaling, endocytosis, access to the cytosol and cytoplasmic transport (Greber, 2002; Meier & Greber, 2003; Ploubidou & Way, 2001; Poranen et al, 2002; Sodeik, 2000). Nuclear import of incoming viral genomes also depends on viral uncoating and in some cases involves an increase of capsid affinity for the NPC (Greber et al, 1994; Whittaker, 2000).

The final steps in the assembly of enveloped viruses occur in the context of a cellular membrane when the nascent particle undergoes a budding reaction that simultaneously generates the viral envelope and releases the free virion. The cellular membrane can be the plasma membrane, leading to virus release directly to the extracellular space, or an intracellular membrane (e.g. the ER, golgi apparatus or endosomal system), in which case the virions are delivered into intracellular vacuoles. In addition, certain viruses and viruslike particles (VLPs) undergo engenous replication and can shuttle their genomes in and out of the nucleus without going through a

complete virus assembly process from which they are released to the extracellular space by a secretory-type mechanism.

It has been reported that WSSV mainly occur in the nuclei of infected lymphoid cells (Wang et al, 2000). The GCs and SGCs were found in hemolymph as the targets for WSSV infection by a TEM study. However, clusters of developing virions and mature virions were only found in the nucleus of SGCs. Even the morphogenesis of WSSV in the infected nucleus of heavily infected SGCs was observed. The nucleus was filled with many empty premature nucleocapsids, most of which were surrounded loosely with an envelope, with both the shell and envelope open at the same end (Wang et al, 2002). Moreover, propagation of WSSV was investigated in primary ovarian cultures from the kuruma shrimp Marsupenaeus *japonicas* (Maeda et al, 2004). Electron microscope observations clearly showed that the replication of WSSV occurred in nuclei of ovarian cells. Based on these evidences, WSSV replication and assembly within the nucleus are crucial step in WSSV propagation. It was reported that VP35 (nucleocapsid protein of WSSV) contained a nuclear translocation signal which mediate the viral DNA to nucleus of WSSV-infected insect cells for viral replication (Chen et al, 2002). It is possible that WSSV uses *Pm*VRP15 for enter or exit from the nucleus. It is common for a virus to use the host machinery for its advantage. For example, *Pm*Rab7 is used in sorting and endocytic trafficking of virus in the host cells (Sritunyalucksana et al, 2006).

*Pm*VRP15 may involve in nuclear import/export of WSSV. To test this hypothesis, ratio of WSSV DNA in nuclear and cytoplasmic fractions of normal and *Pm*VRP15-silenced hemocytes were compared. Knockdown of *Pm*VRP15 resulted in a lower ratio of WSSV copy number in nuclear to cytoplasmic fractions by 9.3 fold, comparison to that of control (Table 4), indicating that *Pm*VRP15 may involve in nuclear entry of WSSV.

For structural study, a large quantity of purified protein is in need. As a result, r*Pm*VRP15 expression was tested in both *S. cerevisiae* and *E. coli* system. *Pm*VRP15 gene was successfully cloned and transformed into *S. cerevisiae* (FGY217). Expression of r*Pm*VRP15 was induced by addition of 20% galactose (final concentration of 2%) for 22 h. However, no major band of protein of 15 kDa

(expected size of r*Pm*VRP15) was detected by SDS-PAGE (Figure 9). This indicates that this *S. cerevisiae* system was not suitable for r*Pm*VRP15 production.

Since a protein with transmembrane helice domain may hinder protein crystallization, soluble parts of *Pm*VRP15 were cloned and expressed in *E. coli* C43 (DE3). N-terminal truncated *Pm*VRP15 contained residue 1-112, while C-terminal truncated *Pm*VRP15 consisted of residue 186-414. Western blot analysis showed that both truncated *Pm*VRP15 proteins were expressed in inclusion bodies at 37 °C (Figure 12 and Figure 13). Although IPTG induction was carried out at 16 °C, C-terminal truncated *Pm*VRP15 was found in inclusion bodies (Figure 13). This indicated that protein expression at low temperature did not help increase truncated *Pm*VRP15 solubility. Since the truncated *Pm*VRP15 proteins cannot be expressed in soluble form, we then focused on working with full-length r*Pm*VRP15.

Full-length r*Pm*VRP15 was expressed in *E. coli* C43 (DE3). The result showed that r*Pm*VRP15 was expressed at 1-3 h after IPTG induction and expressed in the highest level at 2 h post-IPTG induction (Figure 14 and Figure 15). No *Pm*VRP15 band was found after 3 h induction. This suggested that *Pm*VRP15 may be a toxic protein or an unstable protein. In this research, DM (n-decyl-ß-D-maltopyranoside) was used to solubilize r*Pm*VRP15 to ensure it folded correctly. Membrane protein can be solubilize with DM detergent to study their structure and function. Proteins bound to cell membranes have hydrophobic sites buried within the phospholipid bilayers and hydrophilic sites facing toward the water layer. This detergent can interact with the hydrophobic sites of proteins which are then solubilized in the water layer. Moreover, DM detergent does not interfere the bioactivities of target proteins, denature or inactivate target proteins (Prive, 2007). In this study, r*Pm*VRP15 was purified by two steps; Ni-NTA Sepharose™ 6 FF and HiTrap DEAE FF columns, in order to obtain fairly pure protein (Figure 16). Molecular mass of purified r*Pm*VRP15 was determined by MALDI-TOF MS. Recombinant *Pm*VRP15 has a molecular mass of 15,899.9 Da (Figure 17), which is similar to the calculated molecular mass.

CD spectra of r*Pm*VRP15 revealed that the major secondary structure type of r*Pm*VRP15 was alpha-helix, compared to standard protein which known secondary structure. The predicted

secondary structure percentage of r*Pm*VRP15 was 48.45% α-helix and 13.57% β-strand (Figure 18). Helices are common the most common motif in membrane proteins (Cohen & Parry, 1990) and many groups of membrane proteins have alpha-helical secondary structure (Dieckmann & DeGrado, 1997). The fact that purified *Pm*VRP15 adopted secondary structure indicated that the purification procedure used in this study did not destroy protein secondary structure.

SEC revealed that DM detergent is essential for *Pm*VRP15 solubility (Figure 19). *Pm*VRP15 was aggregated in buffer without DM. This may due to high proportion of alpha-helical secondary structure in *Pm*VRP15. AUC analysis revealed that *Pm*VRP15 at 60 μM concentration could possibly form a tetramer (Figure 20).

Protein crystallography can be used to generate atomic resolution structures of protein molecules. In this study, Crystal Screen 1, 2™, PEG/Ion 1, 2 ™, Index™, MembFac™ (Hampton Research), JCSG Core I, II, III, IV Suits, PACT Suits (Qiagen) were used to screen for crystallization conditions of r*Pm*VRP15. Some crystals appeared in 96-well crystallization plates and were tested for X-ray diffraction (Figure 21). However, no well-diffracted protein crystal was found. This may be caused by several factors including small crystals, disorder crystals and influence of detergents. Poor diffraction could be indicative of detergent-mediated crystal contacts.

Reductive alkylation of lysine residues could improve protein crystallization (Kim et al, 2008; Rayment, 1997). However, this did not improve r*Pm*VRP15 crystallization. Further crystallization trials should be done using a complex of r*Pm*VRP15 with its partner protein. In addition, other detergents may be used in protein crystallization.

**6. Conclusions**

In primary hemocyte cultures, the highest *Pm*VRP15 mRNA expression was observed at 48 h post-WSSV infection. Quantitative Real Time RT-PCR showed that silencing of *Pm*VRP15 gene resulted in a reduction of WSSV replication. Confocal laser scanning microscopy revealed that *Pm*VRP15 localized at nuclear membrane of all cell types (GCs, SGCs and HCs). In addition, kn*Pm*VRP15 hemocytes had lower amounts of VP28, compared to knGFP hemocytes. These results indicated that

*Pm*VRP15 is essential for WSSV propagation. Nuclear import/export experiment suggested that *Pm*VRP15 may be involved in nuclear entry of WSSV. Recombinant *Pm*VRP15 was successfully expressed in *E. coli* C43 (DE3) and purified by Ni-NTA and DEAE-FF™ sepharose columns. CD spectrum analysis demonstrated that r*Pm*VRP15 protein contains 48.45% α-helix and 13.57% β-sheet. AUC analysis suggested that *Pm*VRP15 at 60 μM concentration could possibly form a tetramer. Various crystallization screens have been used; however, no *Pm*VRP15 crystal was obtained.

**7. Output**

**Output จากโครงการวิจัยที่ได้รับทุนจาก สกว.**

1. ผลงานตีพิมพ์ในวารสารวิชาการนานาชาติ

   Jaturontakul, K., Supungul, P., Tassanakajon, A., Krusong, K. Molecular characterization of viral responsive protein 15 and its possible role in nuclear import/export of virus in black tiger shrimp *Penaeus mondon*. (submitted)

2. การนำผลงานวิจัยไปใช้ประโยชน์

   - เชิงสาธารณะ (มีเครือข่ายความร่วมมือ)

     สร้างความร่วมมือด้านการศึกษาโครงสร้างสามมิติของโปรตีนกับ Professor Toshio Hakoshima จาก Nara Institute of Science and Technology (NAIST), Japan

   - เชิงวิชาการ (สร้างนักวิจัยใหม่)

     นางสาวกฤษดาพร จาตุรนตกุล (มหาบัณฑิต)

     นางสาวภาสุณีย์ เลาหวุฒิชัย (ปริญญาบัณฑิต)

3. อื่นๆ (เช่น หนังสือ การจดสิทธิบัตร)

   - เสนอผลงาน (โปสเตอร์) และผลงานตีพิมพ์ใน Proceeding

   Jaturontakul, K., Tassanakajon, A. and Krusong, K. “Cloning and expression of viral responsive protein 15 from the black tiger shrimp *Penaeus monodon”* The 29th National Graduate Research Conference, 24-25th October 2013, Mae Fah Luang University, Prince of Songkla University, Thailand, p.935-941.

   - รางวัลเสนอผลงาน (โปสเตอร์) The Bronze Medal Winner for Poster Presentation (Cell and Molecular Biology)

Jaturontakul, K. “Characterization of viral responsive protein 15 and its possible role in nuclear import/export of virus in black tiger shrimp *Penaeus monodon*” The 18th Biological Science Graduate Congress, Faculty of Science, University of Malaya, Kuala Lumpur, Malaysia, 6-8th January 2014.

**Reference**

Brown PH, Schuck P (2006) Macromolecular size-and-shape distributions by sedimentation velocity analytical ultracentrifugation. *Biophysical journal* **90:** 4651-4661

Chen LL, Leu JH, Huang CJ, Chou CM, Chen SM, Wang CH, Lo CF, Kou GH (2002) Identification of a nucleocapsid protein (VP35) gene of shrimp white spot syndrome virus and characterization of the motif important for targeting VP35 to the nuclei of transfected insect cells. *Virology* **293:** 44-53

Cohen C, Parry DA (1990) Alpha-helical coiled coils and bundles: how to design an alpha-helical protein. *Proteins* **7:** 1-15

Dieckmann GR, DeGrado WF (1997) Modeling transmembrane helical oligomers. *Current opinion in structural biology* **7:** 486-494

Durand S, Lightner, D.V. (2002) Quantitative real-time PCR for the measurement of white spot syndrome virus in shrimp. *Journal of fish diseases* **25:** 381-389

Greber UF (2002) Signalling in viral entry. *Cellular and molecular life sciences : CMLS* **59:** 608-626

Greber UF, Singh I, Helenius A (1994) Mechanisms of virus uncoating. *Trends in microbiology* **2:** 52-56

Kim Y, Quartey P, Li H, Volkart L, Hatzos C, Chang C, Nocek B, Cuff M, Osipiuk J, Tan K, Fan Y, Bigelow L, Maltseva N, Wu R, Borovilos M, Duggan E, Zhou M, Binkowski TA, Zhang RG, Joachimiak A (2008) Large-scale evaluation of protein reductive methylation for improving protein crystallization. *Nature methods* **5:** 853-854

Kobayashi M, Kubota M, Matsuura Y (1999) Crystallization and improvement of crystal quality for x-ray diffraction of maltooligosyl trehalose synthase by reductive methylation of lysine residues. *Acta crystallographica Section D, Biological crystallography* **55:** 931-933

Krogh A, Larsson B, von Heijne G, Sonnhammer EL (2001) Predicting transmembrane protein topology with a hidden Markov model: application to complete genomes. *Journal of molecular biology* **305:** 567-580

Louis-Jeune C, Andrade-Navarro MA, Perez-Iratxeta C (2011) Prediction of protein secondary structure from circular dichroism using theoretically derived spectra. . *Proteins* **80:** 374-381

Maeda M, Saitoh H, Mizuki E, Itami T, Ohba M (2004) Replication of white spot syndrome virus in ovarian primary cultures from the kuruma shrimp, Marsupenaeus japonicus. *Journal of virological methods* **116:** 89-94

Meier O, Greber UF (2003) Adenovirus endocytosis. *The journal of gene medicine* **5:** 451-462

Newstead S, Kim H, von Heijne G, Iwata S, Drew D (2007) High-throughput fluorescent-based optimization of eukaryotic membrane protein overexpression and purification in *Saccharomyces cerevisiae*. *Proceedings of the National Academy of Sciences of the United States of America* **104:** 13936-13941

Pfaffl MW (2001) A new mathematical model for relative quantification in real-time RT-PCR. *Nucleic acids research* **29:** e45

Ploubidou A, Way M (2001) Viral transport and the cytoskeleton. *Current opinion in cell biology* **13:** 97-105

Poranen MM, Daugelavicius R, Bamford DH (2002) Common principles in viral entry. *Annual review of microbiology* **56:** 521-538

Prive GG (2007) Detergents for the stabilization and crystallization of membrane proteins. *Methods* **41:** 388-397

Rayment I (1997) Reductuve alkylation of lysine residues to alter crystallization properties of proteins. *Methods Enzymol* **276:** 171-179

Rypniewski WR, Holden HM, Rayment I (1993) Structural consequences of reductive methylation of lysine residues in hen egg white lysozyme: an X-ray analysis at 1.8-A resolution. *Biochemistry* **32:** 9851-9858

Schuck P (2000) Size-distribution analysis of macromolecules by sedimentation velocity ultracentrifugation and lamm equation modeling. *Biophysical journal* **78:** 1606-1619

Sodeik B (2000) Mechanisms of viral transport in the cytoplasm. *Trends in microbiology* **8:** 465-472

Sritunyalucksana K, Wannapapho W, Lo CF, Flegel TW (2006) *Pm*Rab7 is a VP28-binding protein involved in white spot syndrome virus infection in shrimp. *J Virol* **80:** 10734-10742

Vatanavicharn T, Prapavorarat A, Jaree P, Somboonwiwat K, Tassanakajon A (2014) PmVRP15, a novel viral responsive protein from the black tiger shrimp, Penaeus monodon, promoted white spot syndrome virus replication. *PLoS One* **9:** e91930

Wang CH, Yang HN, Tang CY, Lu CH, Kou GH, Lo CF (2000) Ultrastructure of white spot syndrome virus development in primary lymphoid organ cell cultures. *Diseases of aquatic organisms* **41:** 91-104

Wang YT, Liu W, Seah JN, Lam CS, Xiang JH, Korzh V, Kwang J (2002) White spot syndrome virus (WSSV) infects specific hemocytes of the shrimp *Penaeus merguiensis*. *Diseases of aquatic organisms* **52:** 249-259

Whittaker GR, Kann, M., and Helenius, A. (2000) Viral entry into the nucleus. . *Annu Rev Cell Dev Biol* **16:** 627-651

# Molecular Characterization of Viral Responsive Protein 15 and Its Possible Role in Nuclear Import/Export of Virus in Black Tiger shrimp *Penaeus monodon*

Krisadaporn Jaturontakul, M.Sc.[a]
Premruethai Supungul, Ph.D.[a,b]
Anchalee Tassanakajon, Ph.D.[a]
Kuakarun Krusong, Ph.D.[a, ✉]

[a] Center of Excellence for Molecular Biology and Genomics of Shrimp, Department of Biochemistry, Faculty of Science,
Chulalongkorn University, Bangkok 10330, Thailand

[b] National Center for Genetic Engineering and Biotechnology (BIOTEC),
National Science and Technology Development Agency (NSTDA),
Pathumthani 12120, Thailand

✉ Correspondence:
Kuakarun Krusong, Ph.D. (Kuakarun.K@chula.ac.th)
Department of Biochemistry, Faculty of Science,
Chulalongkorn University, Bangkok 10330, Thailand
Tel: +66 (0)2 218 5413

**Abbreviations** VRP15, viral responsive protein 15; *Pm*, *Penaeus monodon*; WSSV, white spot syndrome virus

**Abstract**

A viral responsive protein 15 (*Pm*VRP15) has been identified from suppression subtractive hybridization library at the early (24 h) and late phase (48/72h) of WSSV infection. *Pm*VRP15 was highly up-regulated in the hemocyte of white spot syndrome virus-infected *Penaeus monodon*. A protein domain prediction indicated that *Pm*VRP15 consisted of a transmembrane helix. In primary hemocyte cultures, *Pm*VRP15 mRNA expression was up-regulated about 1.1, 2.6, 3.6, 6.7 and 4.1 fold at 6, 12, 24, 48 and 72 h post-WSSV infection, respectively. After *Pm*VRP15 gene silencing by RNA interference (RNAi), VP28 transcript was reduced by 4.2 fold at 24 h post WSSV-infection, compared to normal WSSV-infected *P. monodon* hemocytes. These results suggested that *Pm*VRP15 is important to WSSV propagation. Confocal laser scanning microscopy study revealed that *Pm*VRP15 localized at the nuclear membrane. In this study, subcellular fractionation of WSSV-infected hemocytes showed that *Pm*VRP15 was probed in soluble nuclear and chromatin-bound fractions. Taken together, *Pm*VRP15 may function in nucleus as a part of membrane protein or related with membrane protein. It is possible that *Pm*VRP15 involves in nuclear import/export of WSSV. To test this hypothesis, ratio of WSSV DNA in nuclear and cytoplasmic fractions of normal and *Pm*VRP15-silenced hemocytes were compared. Knockdown of *Pm*VRP15 resulted in a lower ratio of WSSV copy number in nuclear to cytoplasmic fractions by 9.3 fold, compared to that of control, indicating that *Pm*VRP15 may involve in nuclear entry of WSSV. Recombinant *Pm*VRP15 was expressed in *Escherichia coli* C43 (DE3) and purified by Ni-NTA Sepharose™ 6 FF and HiTrap DEAE FF columns, respectively. MALDI-TOF MS revealed that the molecular weight of *Pm*VRP15 is 15.899 kDa. Circular

dichroism spectrum analysis revealed that *Pm*VRP15 contains 48.45 % of alpha-helix and 13.57 % of beta-sheet.

**Keywords** *Penaeus monodon*, Viral responsive protein 15, White spot syndrome virus, WSSV

**Introduction**

The cultivation of penaeid shrimp is an important economic activity in the world. However, this industry has been suffered from viral and bacterial diseases worldwide. White spot syndrome virus (WSSV) is a major viral pathogens of *P. monodon* which cause white spot syndrome. WSSV is the type specie of the genus Whispovirus in the viral family Nimaviridae, containing a circular double-stranded DNA of about 305 kb, and is an enveloped rod-shaped particle with a single filamentous appendage-like tail at one end of the nucleocapsid (Yang et al. 2001, Vlak 2004). The average size of the virus is about 298 ± 21 nm long and 107 ± 8 nm in diameter (Wang et al., 1997). WSSV is a lytic virus that replicates and assembles in the nucleus. At the late stage of infection, the infected nuclei/cells are lysed, causing the infected tissues to become severely damaged and necrotic.

Viral Responsive Protein 15, *Pm*VRP15, was found to be highest up-regulated gene ever reported in the hemocytes of WSSV-infected *P. monodon* using suppression subtractive hybridization approach (Vatanavicharn et al. 2014). The predicted open reading frame of *Pm*VRP15 encodes for a deduced 137 amino acid protein containing a putative transmembrane helix. Tissue distribution analysis showed that *Pm*VRP15 transcript was mainly expressed in the hemocytes of shrimp. *Pm*VRP15 was found in all three types of hemocytes and *Pm*VRP15 was localized in the cytoplasm near to the nuclear membrane. Interestingly, *Pm*VRP15 and VP28 protein expression were found in the same hemocytes at the late infection phase (48 hpi) of viral infection. Thus, the expression of *Pm*VRP15 in *P. monodon* hemocytes appears to be linked to a response to the acute phase of WSSV infection. *Pm*VRP15 is likely to be a nuclear membrane protein and that it acts as a part of WSSV propagation pathway (Vatanavicharn *et al.* 2014).

In this study, the function of *Pm*VRP15 in response to WSSV has been studied *in vitro*. The expression of *Pm*VRP15 gene upon WSSV infection has been examined in primary hemocyte cell culture using Real-time PCR. Then, effects of *Pm*VRP15 on WSSV propagation have been studied by RNA interference. After WSSV infection, VP28 transcripts of normal and *Pm*VRP15-silenced hemocytes have been compared by Real-time PCR. A possible role of *Pm*VRP15 in nuclear import/export has been further investigated by measuring WSSV copy number in nuclear and cytoplasmic fractions. Moreover, molecular mass and secondary structure of recombinant *Pm*VRP15 have been analyzed by MALDI-TOF mass spectrometry and circular dichroism spectroscopy, respectively.

**Materials and Methods**

*2.1 Shrimp*

Juveniles black tiger shrimp, *P. monodon*, of about 10-15 g bodyweight were obtained from shrimp farm in Nakhon Si Thammarat Province, Thailand. The animals were acclimated in laboratory tanks at ambient temperature (28 ± 4 °C), and maintained in aerated water with a salinity of 20 ppt for at least 7 days before use.

*2.2 Preparation of WSSV stock*

The gill tissue from WSSV-infected moribund shrimp was collected for the purification of viral particles. The purification method was slightly modified from (Xie *et al.* 2005). Gill tissue was homogenized in TNE buffer (50 mM Tris-HCl pH 8.5, 400 mM NaCl and 5 mM EDTA) and, then, centrifuged at 3,500× g for 15 min at 4 °C. The supernatant was filtrated with MILLEX®-HP Filter Unit 0.45 µm (Merck Millipore) and centrifuged at 30,000 xg for 30 min at 4 °C to pellet the virions. The pellet was rinsed with TM buffer (50 mM Tris-HCl pH 7.5 and 10 mM $MgCl_2$) and centrifuged at 3,500 xg for 10 min at 4 °C. Subsequently, the pellet was resuspended in TM buffer and, then, supernatant was subjected to centrifugation at 30,000× g for 30 min at 4 °C. The pellet was then suspended in TM buffer and divided into aliquots and stored at -80 °C until use.

*2.3 Primary Shrimp hemocyte cultures*

Hemolymph was drawn from each shrimp (~10-15 g body weight) using a sterile 1 ml syringe with 500 µl of anticoagulant, pH 5.6 (0.82% (w/v) sodium chloride, 0.55% (w/v) citric acid, 1.98% (w/v) glucose and 0.88% (w/v) sodium citrate; adjusted to pH 5.6 with sodium hydroxide solution). The hemolymph-

anticoagulant mixture was immediately centrifuged at 800 x g for 10 min at 4 °C to separate the hemocytes from the plasma. The hemocyte pellet was resuspended in 1 ml of L-15 culture medium (2x Leibovitz L-15 medium (Gibco) supplemented with 20% (v/v) fetal bovine serum (FBS), 1% (w/v) glucose, 0.4% (w/v) sodium chloride, 100 IU/ml penicillin and 100 µg/ml streptomycin; pH 7.6; adjusting the osmotic pressure to 750 ± 15 mOsm/kg with sodium chloride solution).

The number of hemocyte in the cell suspension was counted by a hematocytometer. Cell concentration was adjusted to $10^6$ cells per ml per well by L-15 fresh medium to obtain a final volume of 400 µl per well. The 24-well plate was then incubated at 28 °C for 24 h, prior to be used in the experiments.

*2.4 Determination of PmVRP15 mRNA expression in response to WSSV infection in shrimp primary hemocyte culture by RT-PCR and Real-time PCR*

After pre-treatment of primary hemocyte cultures as above, 400 µl of L-15 culture medium was removed from each well and replaced with 400 µl of fresh L-15 culture medium with or without 50 µl of the diluted WSSV solution (~15,000 viral copies/µl). Then, hemocyte cultures were re-incubated at 28 °C. Total RNA was extracted from the hemocytes at 0, 6, 12, 24, 48 and 72 h post-WSSV infection using the TRI Reagent® (Molecular Research Center) followed by DNase I, RNase-free (Thermo scientific) treatment, and used for single-stranded cDNA synthesis by the First Strand cDNA Synthesis Kit (Thermo Scientific).

The transcription level of target genes was identified by RT-PCR using an equal amount of cDNA template with gene-specific primers (Table 1). The Elongation factor-1 alpha (EF-1α) was used as an internal control. The PCR conditions consisted of 94 °C for 3 min, followed by 33 cycles (for *Pm*VRP15) or 28

cycles (for EF-1α) cycles of 95 °C for 30 sec, 58 °C for 30 sec and 72 °C for 30 sec, and a final extension at 72 °C for 5 min. The PCR products were analyzed by 1.5% (w/v) agarose gel electrophoresis and visualized using Gel Documentation System (Syngene). The differential expression level of *Pm*VRP15 was reported as relative to EF-1α.

The expression level of *Pm*VRP15 and EF-1α gene was further analyzed by quantitative real time RT-PCR (qRT-PCR). *Pm*VRP15 and EF-1α specific primers for qRT-PCR were shown in Table 1. The qRT-PCR was performed using the CFX96™ Real-Time PCR Detection System (Bio-Rad). The PCR condition was performed as follows: 95 °C for 30 sec, followed by 40 cycles of 95 °C for 5 sec, 58 °C for 5 sec and 60 °C for 5 sec. The experiment was carried out in triplicate. The threshold cycle ($C_T$) for each sample was analyzed by a mathematical model described by (Pfaffl, 2001). The data were shown as means ± standard deviations (SD). Statistical analysis was done using the one-way ANOVA followed by post hoc test (Duncan's new multiple range test). Data differences were considered significant at $P < 0.05$ (*), $P < 0.01$ (**).

*2.5 Production of PmVRP15 and GFP dsRNA*

Gene silencing was used to study the important role of *Pm*VRP15 in the WSSV-infection in primary hemocyte cell culture. The dsRNA *Pm*VRP15 was used to knockdown *Pm*VRP15 transcript prior to WSSV infection. The *Pm*VRP15 dsRNA and GFP dsRNA (control group) were synthesized using T7 RiboMAX™ Express Large Scale RNA Production System (Promega) following the manufacturer protocol.

*Pm*VRP15 and Green fluorescent protein (GFP) DNA templates with a single T7 promoter at the 5' ends were PCR amplified from the *Pm*VRP15-recombinant

plasmid and the pEGFP-1 vector (Clontech) by specific primer sets, respectively (Table 1). PCR was performed as followed : 94 °C for 3 min, 30 cycles of 94 °C for 30 sec, 57 °C for 30 sec and 72 °C for 30 sec, and then a final extension at 72 °C for 5 min. Subsequently, *Pm*VRP15 dsRNA was produced using T7 RiboMAX$^{TM}$ Express Large Scale RNA Production System (Promega) to produce two complementary ssRNAs according to the manufacturer's instruction. Then, equal amounts of each of the complementary ssRNAs were mixed together and incubated at 70 °C for 10 min, and slowly cooled down at room temperature to allow a formation of dsRNA. The *Pm*VRP15 dsRNA solution was treated with 2 units of RQ1 RNase-free DNase (Promega) at 37 °C for 15 min to remove DNA template, and then purified by standard phenol-chloroform extraction.

*2.6 Investigation of VP28 transcript level after PmVRP15 silencing in WSSV-infected hemocytes by RT-PCR and quantitative Real-time PCR*

After pre-treatment of primary hemocyte cultures as above, Fresh L-15 medium supplemented with 20% fetal bovine serum was replenished. The dsRNA was pre-incubated with histone H2A (calf thymus, type II-A; Sigma) for 10 min at RT (Liu et al., 2006) before used.

The hemocyte cell cultures, divided into 3 groups, were incubated with 50 µl of L-15 medium with or without, 20 µg/well of GFP dsRNA or *Pm*VRP15 dsRNA. After 12 h, 50 µl of L-15 medium with or without, GFP dsRNA (10 µg/well) and *Pm*VRP15 dsRNA (10 µg/well) were added along with 50 µl of the diluted WSSV solution (~15,000 viral copies/µl) and incubated at 27 °C. At 24 h post-WSSV infection, hemocyte cells were harvested and total RNA was extracted from hemocytes using the TRI Reagent® (Molecular Research Center) followed by DNase

I, RNase-free (Thermo scientific) treatment, and then single-stranded cDNA was synthesized with the First Strand cDNA Synthesis Kit (Thermo Scientific) and cDNA was used to analyze VP28 mRNA expression by RT-PCR with EF-1α as an internal reference.

The expression of VP28, *Pm*VRP15 and EF-1α genes were analyzed by RT-PCR using gene specific primers (Table 1). The reaction were carried out using the following conditions: an initial denaturation at 94 °C for 5 min, followed by 30 cycles of denaturation at 94 °C for 30 s, annealing at 60 °C for 30 s, elongation at 72 °C for 30 s, and the final extension at 72 °C for 10 min. The PCR reactions were analyzed by agarose gel electrophoresis and visualized by gel documentation system (SynGene).

The expression level of VP28 and EF-1α gene was also analyzed by quantitative real time RT-PCR (qRT-PCR). VP28 and EF-1α specific primers were used for qRT-PCR are shown in Table 1. The qRT-PCR was performed using the CFX96™ Real-Time PCR Detection System (Bio-Rad). The PCR profile was as follows: 95 °C for 30 sec, followed by 40 cycles of 95 °C for 5 sec, 58 °C for 5 sec and 60 °C for 5 sec. Each sample was done in triplicate. The threshold cycle ($C_t$) for each sample was analyzed by a mathematical model described by (Pfaffl, 2001). The data were shown as means ± standard deviations (SD). Statistical analysis was done using the one-way ANOVA followed by post hoc test (Duncan's new multiple range test). Data differences were considered significant at $P < 0.05$.

Comparative $C_T$ method was used to compare the gene expression in two different samples. The fold change of gene expression was calculated using following formula.

Fold change = 2- $\Delta\Delta C_T$

$\Delta\Delta C_T$ = [($C_T$ gene of interest - $C_T$ internal control) sample A - ($C_T$ gene of interest - $C_T$ internal control) sample B)]

*2.7 Purification of primary antibody*

Rabbit polyclonal antiserum against the purified r(His)6-*Pm*VRP15 protein (2 mg) was a gift from Dr. Tipachai Vatanavicharn, Chulalongkorn University. To purify the IgG antibody form anti-serum standard protocol, protein A Sepharose CL-4B (GE Healthcare) was used according to the manufacturer. The protein A Sepharose CL-4B bead was applied into the column and washed with 10 volumes of PBS. Anti-serum was loaded into the column and incubated at RT for 10 min. After washing with PBS to remove non-specific proteins, IgG antibody was eluted with elution buffer (100 mM glycine pH 2.5) and immediately neutralized with 1 M Tris pH 9.5. Then, eluted primary antibody was added with 0.02% Sodium azide as preservative to prevent microbial contamination.

*2.8 Visualization of normal and PmVRP15-knockdown hemocyte-infected by WSSV using confocal immunofluorescence microscopy*

Twenty-five µl of 150 mM sodium chloride containing GFP dsRNA (5 µg/g shrimp) or *Pm*VRP15 dsRNA (10 µg/g shrimp) was injected into each shrimp (~10 g body weight). After 24 h, the shrimp were injected with 25 µl of 150 mM sodium chloride containing GFP dsRNA (5 µg/g shrimp) or *Pm*VRP15 dsRNA (5 µg/g shrimp), along with 30 µl of the diluted WSSV solution (~ 4 x$10^3$ viral copies). At 48 h post-injection, hemolymph was immediately fixed with of 4% (w/v) paraformaldehyde for 10 min. Hemocytes were collected by contrifugating 800 x g for 10 min and washed three times with PBS, pH 7.4, and then immersed in PBS, pH

7.4, and kept at 4 °C until the next treatment. A hemocytometer was used to count the number of hemocytes and to make $1x10^6$ cells/ml of hemocytes.

Hemocytes were attached onto a polylysine coated microscope slide (Polysine slides, Thermo Scientific) using cytospin centrifugation. The slide was washed by PBS for 5 min and later covered by 200 µl of 0.1% (v/v) Triton-X 100 in PBS for 5 min at RT to permeabilize the hemocyte membrane. After rinsing the slide in PBS for 5 min, it was immersed in 200 µl of blocking solution (10% (v/v) FBS in PBS) for 1 h at RT followed by washing in PBS. The fixed hemocytes were probed with a 1:500 dilution of purified rabbit anti-*Pm*VRP15 polyclonal antibody and 1:100 dilution of mouse anti-VP28 polyclonal antibody in PBS, containing 1% (v/v) FBS at RT for 3 h. Then, washed three times with PBS, and then incubated with a 1:500 dilution of Alexa Fluor 488 goat anti-rabbit IgG antibody (Invitrogen) and Alexa Fluor® 568 goat anti-mouse IgG antibody (Invitrogen) in PBS at RT for 1 h in the dark, and washed three times with PBS. Subsequently, the nucleus was stained with a 1: 1500 dilution of TO-PRO-3 iodide (Invitrogen) in PBS, at RT for 10 min in the dark, and washed three times with PBS. The cover slips contained the stained and fixed hemocyte samples were then coated with Prolong Gold Antifade Reagent (Invitrogen). Next, the slide was visualized under a confocal laser scanning microscope (CLSM).

*2.9 Protein localization of PmVRP15 by subcellular protein fractionation*

After pre-treatment of primary hemocyte cultures as above, Fresh L-15 medium supplemented with 20% fetal bovine serum was replenished. The hemocyte cell cultures were incubated with 50 µl of the diluted WSSV solution (~15,000 viral copies/µl) and incubated at 27 °C. For 48 h post-WSSV infection, total protein was extracted from hemocytes using Subcellular fractionation kit for cultured cells

(Thermo Scientific). Cytoplasmic, membrane, soluble nuclear, chromatin-bound and cytoskeletal fractions were extracted. The total protein concentration of each fraction was determined using BCA protein assay and 10 μg of proteins were loaded in each lane. The result was analyzed by Western blotting. Each fraction was probed with anti-*Pm*VRP15 as primary antibody (1:1000) at 37 °C for 3 h. After washing with PBST, membrane was probed with alkaline phosphatase-conjugated goat anti-rabbit IgG (1:10,000).

*2.10 Quantification of WSSV copy number in normal and PmVRP15 silencing hemocytes after WSSV infection*

*Pm*VRP15 was located near or at nuclear membrane and it may involve in viral entry or viral shedding to or from the nucleus. Thus, there are two main hypotheses when it comes to explaining. First, if *Pm*VRP15 involves in viral entry (Figure 1A), after silencing *Pm*VRP15 gene, a lot of WSSV will be found in cytoplasmic fraction as WSSV cannot enter into nucleus. Thus, the ratio of DNA virus (WSSV) in nucleus to cytoplasmic fraction of *Pm*VRP15 silencing will be lower than that of control (GFP silencing).

However, if *Pm*VRP15 involves in viral exit (Figure 1B), after silencing *Pm*VRP15 gene, a lot of WSSV will be found in nuclear fraction since WSSV can enter into nucleus to replicate but cannot leave the nucleus. Thus, the ratio of DNA virus (WSSV) in nucleus to cytoplasmic fraction of *Pm*VRP15 silencing will be higher than that of control (GFP silencing).

After pre-treatment of primary hemocyte cultures as above, Fresh L-15 medium supplemented with 20% fetal bovine serum was replenished. The dsRNA

was pre-incubated with histone H2A (calf thymus, type II-A; Sigma) for 10 min at RT (Liu et al., 2006) before used.

The hemocyte cell cultures, divided into 2 groups, were incubated with 50 µl of GFP dsRNA (20 µg/well) or *Pm*VRP15 dsRNA (20 µg/well). After 12 h, 50 µl of GFP dsRNA (10 µg/well) and VRP15 dsRNA (10 µg/well) were added, along with 50 µl of the diluted WSSV solution (~15,000 viral copies/µl) and incubated at 27 °C. For 24 h post-WSSV infection, total DNA was extracted from hemocytes using Subcellular fractionation kit for cultured cells (Thermo Scientific). The cytoplasmic and nuclear fractions were separated and sent to Charoen Pokphand Foods PCL for the determination of the WSSV copy number in each fraction by Real-time PCR with the WSSV1011F/WSSV1079R primers, as described by (Durand, 2002), using an ABI7000 Sequence Detection System. The data was carried out in triplicate and WSSV recombinant plasmid (known copy number) was used as the standard for quantification.

*2.11 Confirmation of cross contamination in cytoplasmic and nuclear fractions of PmVRP15 silencing and control (GFP silencing) using Western blotting analysis*

To confirm cytoplasmic and nuclear fractions are no cross-contaminated, anti-Nuclear Pore Complex (NPC) antibody was used for Western blotting. NPC was found in nuclear fraction only. Cytoplasmic and nuclear fractions were extracted from cultured cells and total protein concentration of each fraction was determined using BCA protein assay. Ten µg of proteins were loaded in each lane. The result was analyzed by Western blotting (Pierce® Fast Western Blot Kit, SuperSignal® West Femto Substrate). Each fraction was probed with anti-NPC as primary antibody (1:1000) at 37 °C for 2 h. After washing with washing buffer, membrane was probed

with Fast Western Mouse optimized HRP-labeled secondary antibody, Femto. Membrane was soaked and shaked for 1 hour at RT. Wash 3 times with wash buffer for 10 min/time, working solution (Luminol/Enhancer solution 1 : 1 Peroxide reagent) was added to membrane for 15 min at RT. The excess buffer was removed and membrane was placed on a plastic wrap. Then, signal was detected using Amersham™ Hyperfilm ECL (GE Healthcare).

*2.12 Production of rPmVRP15 in E. coli expression system*

The *Pm*VRP15-recombinant pET22b(+) was a gift from Dr. Tipachai Vatanavicharn, Chulalongkorn University. The *Pm*VRP15-recombinant pET22b(+) was transformed into *E. coli* C43 (DE3) competent cells by heat shock method and transformants were grown on LB agar containing 100 µg/ml ampicillin at 37°C overnight. A single colony of transformed *E. coli* was grown in LB medium containing 100 µg/ml ampicillin at 37 °C overnight with agitation at 250 rpm. The overnight culture was diluted 1:100 in fresh LB medium supplemented with 100 µg/ml ampicillin and grown until an $OD_{600}$ of the cultures reached 0.6. Protein expression was induced by addition of IPTG to final concentration of 1 mM. The cells were harvested at 0, 1, 2, 3, 4, 5 and 6 hour post-induction by centrifugation at 8,000 xg for 10 min at 4 °C. The overexpression of r*Pm*VRP15 was analyzed by SDS-PAGE and Western blotting.

*2.13 Membrane preparation of the rPmVRP15*

The *Pm*VRP15-recombinant pET22b(+) *E. coli* was grown in LB medium containing 100 µg/ml ampicillin at 37 °C overnight with agitation at 250 rpm. The culture was diluted 1:100 in fresh LB medium supplemented with 100 µg/ml

ampicillin and grown until an $OD_{600}$ of the cultures reached 0.6. Cells were harvested at 1 h post-induction by centrifugation at 8,000 xg for 10 min at 4 °C, then the cells were resuspended in 50 mM Tris-HCl buffer, pH 7.0 containing complete Protease inhibitor cocktail tablets (Roche). The cell suspension was disrupted by three rounds of freeze/thaw followed by sonication. Cells were sonicated 10 rounds of at 35% amplitude, pulse on 2 sec, pulse off 3 sec for 40 sec/round. Supernatant was collected after centrifugation at 8,000 xg 4 °C for 20 min and membrane r*Pm*VRP15 protein was obtained by centrifugation at 100,000 xg 4 °C for 1 h. Membrane r*Pm*VRP15 protein was homogenized in 50 mM Tris-HCl buffer, pH 7.0 containing protease inhibitor tablet by homogenizer.

*2.14 Purification of the rPmVRP15 protein*

Membrane r*Pm*VRP15 protein was solubilized in solubilization buffer (50 mM Tris-HCl, pH 7, 20 mM Imidazole, 300 mM NaCl, 20% glycerol and 1% n-decyl-ß-d-maltopyranoside, DM) at 4 °C overnight. The r*Pm*VRP15 solubilized protein was purified using the affinity chromatography by Ni-NTA Sepharose™ 6 Fast Flow (GE Healthcare). The purified r*Pm*VRP15 was dialyzed against dilution buffer (10 mM Tris-HCl, pH 7, 2.5% glycerol and 0.07% DM).

The r*Pm*VRP15 protein was further purified by weak anion exchanger chromatography, HiTrap DEAE Fast Flow. The purified r*Pm*VRP15 was analyzed by 15% SDS-PAGE. The purified r*Pm*VRP15 was confirmed by Western blot analysis. The purified protein was concentrated using centricon columns (Millipore) with a 10 kDa cut-off membrane. Protein concentration of r*Pm*VRP15 was determined by Pierce® BCA Protein Assay Kit (Thermo scientific).

*2.15 Molecular mass analysis of rPmVRP15 using MALDI-TOF Mass spectrometry (MALDI-TOF MS)*

To determine the molecular weights of r*Pm*VRP15, purified r*Pm*VRP15 was sent to Mahidol University for MALDI-TOF MS analysis. The commercially available MALDI MS Autoflex Speed linear and Autoflex TOF/TOF (Bruker Daltonics) were used in these experiments. MALDI-TOF MS analysis and calibration for quantification. Mass spectrometric analysis was carried out on a Voyager DE-Pro MALDI-TOF MS instrument (Applied Biosystems) in linear positive mode. After time-delayed extraction, the ions were accelerated to 20 kV for TOF mass spectrometric analysis. A total of 400 laser shots were acquired and signal averaged per mass spectrum.

*2.16 Determination of secondary structure of rPmVRP15 using Circular Dichroism (CD) spectroscopy*

To determine investigate the secondary structure of r*Pm*VRP15, circular dichroism (CD) spectroscopy was used. Circular dichroism studies were carried out with a JASCO J-715 CD Spectropolarimeter with temperature controller using a 1 mm optical cuvette. The (+)-10-camphorsulfonic acid (CSA) was used as calibration standard before measuring CD spectrum. Spectra were recorded between 180-320 nm using a bandwidth of 2 nm and a response time of 2 sec with 50 mm/min scanning speed. Each spectrum was the average of three scans and background was subtracted with the spectrum of 10 mM Phosphate buffer pH 7.0 (blank). Purified r*Pm*VRP15 proteins were dialyzed against 10 mM phosphate buffer pH 7.0. The mean residue ellipticity (MRE) was calculated according to the following formula: MRE = E x

100/(c x d x N) [deg $cm^2$ $dmol^{-1}$] (E: ellipticity in deg, c: concentration in mol $L^{-1}$, d: path length in cm, N: number of amino acid residues).

CD spectra of r*Pm*VRP15 revealed the major secondary structure type of r*Pm*VRP15 compared to standard protein which known secondary structure (http://www.ogic.ca/projects/k2d3/).

**Results**

*3.1 PmVRP15 mRNA expression in unchallenged- and WSSV-challenged shrimp*

In primary hemocyte cultures, *Pm*VRP15 mRNA levels in response to WSSV infection. *Pm*VRP15 transcripts in WSSV-infected hemocytes were up-regulated at 6, 12, 24, 48 and 72 h post-WSSV infection compared to non-infected hemocytes (Figure 2).

*3.2 Quantitative analysis of PmVRP15 mRNA expression in response to WSSV infection*

In shrimp primary hemocyte cell cultures, *Pm*VRP15 transcript levels were evaluated by Real-time PCR. The results clearly demonstrated that *Pm*VRP15 expression levels in WSSV-infected hemocytes was up-regulated when compared to non-infected hemocytes. *Pm*VRP15 mRNA expression was up-regulated by about 1.1, 2.6, 3.6, 6.7 and 4.1 fold at 6, 12, 24, 48 and 72 h post-infection, respectively (Figure 3). These results suggest that *Pm*VRP15 transcript is up-regulated in WSSV infection.

*3.3 In vitro double strand RNA-mediated knockdown of PmVRP15 gene expression resulted in reduction of WSSV propagation by RT-PCR*

In primary hemocyte cultures, knockdown of *Pm*VRP15 gene in WSSV-infected hemocytes resulted in the reduction of VP28 gene expression (Figure 4).

*3.4 In vitro double strand RNA-mediated knockdown of PmVRP15 gene expression resulted in reduction of WSSV propagation by Real-time PCR*

Viral gene, VP28 transcript levels were evaluated by Real-time PCR. The results demonstrated that VP28 mRNA expression was decreased in shrimp hemocytes after *Pm*VRP15 gene silencing via RNAi. VP28 transcript was reduced by about 4.17 fold (84.29%) at 24 h post WSSV-infection compared to that of normal *P. monodon* hemocytes infected by WSSV (Figure 5). This result suggests that *Pm*VRP15 is important for WSSV propagation.

*3.5 PmVRP15 is localized in three types of WSSV-infected hemocytes*

Hemocytes collected from *Pm*VRP15-silenced and GFP-silenced of WSSV-infected shrimp were used in this study. The bright field image revealed three types of hemocytes, granular cells (GC) semi-granular cells (SGC) and hyaline cells (HC). Similar to previous study (Vatanavicharn et al., 2014), *Pm*VRP15 protein expression was observed in all three types of hemocytes at 48 h post WSSV infection. *Pm*VRP15 protein was located at the edge of nucleus, or possible at the nuclear membrane of the cell. This is in agreement with the fact that *Pm*VRP15 was predicted to contain a transmembrane helix.

*Pm*VRP15 and VP28 protein were observed as green fluorescence and red fluorescence, respectively. Nuclear DNA of hemocytes was stained with TO-PRO-3 iodine and adjusted to show as blue (Figure 6). Hemocytes of kn*Pm*VRP15 showed lower amounts VP28 than those of knGFP cells. This indicated that knockdown of *Pm*VRP15 reduced WSSV propagation.

In *Pm*VRP15-silenced of WSSV-infected hemocytes, the green fluorescent signal of *Pm*VRP15 was still observed, but the intensity of the signal was lower than that observed in GFP-silenced hemocytes. This indicated *Pm*VRP15 was not completely silenced at 48 hpi, the time point at which *Pm*VRP15 was highestly expressed (Figure 3).

*3.6 Protein localization of PmVRP15 by subcellular protein fractionation in WSSV-infected hemocyte cultures using subcellular fractionation kit*

The hemocyte cultures were infected with WSSV and incubated at 27 °C. At 48 h post-WSSV infection, total protein was extracted from hemocytes using subcellular fractionation kit for cultured cells (Thermo Scientific). Cytoplasmic, membrane, soluble nuclear, chromatin-bound and cytoskeletal fractions were extracted from WSSV-infected hemocyte cultures. The concentration of total protein in each fraction were determined using BCA protein assay and 10 µg of proteins were loaded in each lane. The result was analyzed by Western blotting. *Pm*VRP15 protein was found in soluble nuclear, and chromatin-bound fractions (Figure 7). This indicated that *Pm*VRP15 is a nuclear localized protein.

*3.7 Quantitation of WSSV copy number in nuclear and cytoplasmic fractions of normal and knPmVRP15 hemocyte cultures after WSSV infection*

The quantities of WSSV in each fraction were quantified by Real time RT-PCR with EF-1α as an internal reference. The ratio of DNA virus (WSSV) in nucleus to cytoplasmic fraction of *Pm*VRP15 silenced hemocyte cultures was compared to that of the control (GFP silencing). In the case that *Pm*VRP15 involved in nuclear entry, the ratio of WSSV DNA in nucleus to cytoplasm of *Pm*VRP15-silenced hemocytes would be lower than that of control. However, if *Pm*VRP15 involved in nuclear exit, the ratio of WSSV DNA in nucleus to cytoplasm would be expected to be higher in *Pm*VRP15-silenced hemocyte cells, compared to that of control.

Table 2 shows the ratio of WSSV DNA in nuclear to cytoplasmic fractions of ds*Pm*VRP15 and dsGFP samples. The experiment was carried out in triplicate and EF-1α was used for normalization of WSSV DNA quantification. The result showed that the ratio of DNA virus (WSSV) in nucleus to cytoplasmic fraction of *Pm*VRP15-silenced was lower than that of control (GFP-silenced hemocytes) by 9.28 fold. This suggested that *Pm*VRP15 plays a role in nuclear entry of WSSV.

*3.8 No cross contamination in cytoplasmic and nuclear fractions of WSSV-infected PmVRP15 silenced and control*

Cytoplasmic and nuclear fractions of WSSV-infected *Pm*VRP15-silenced and GFP-silenced hemocytes were subjected to Western blotting using Nuclear Pore Complex (NPC) antibody as primary antibody. The result showed that NPC protein

was only observed in nuclear fractions of *Pm*VRP15-silenced and GFP-silenced hemocytes. In contrast, NPC protein was not observed in cytoplasmic fractions of *Pm*VRP15- silenced and GFP-silenced hemocytes. This indicated that there was no cross-contamination between cytoplasmic and nuclear fractions (Figure 8). Thus, cytoplasmic and nuclear fractions were sent to Charoen Pokphand Foods PCL for determination of the WSSV copy number by Real-time PCR.

*3.9 Expression and purification of rPmVRP15 in E. coli expression system*

Full-length r*Pm*VRP15 was produced in the *E. coli* C43 (DE3) induced by adding IPTG to final concentration of 1 mM and then incubated for 0, 1, 2, 3, 4, 5 and 6 h at 37 °C. Expression of r*Pm*VRP15 was analyzed by SDS-PAGE (Figure 9A). The result showed that the r*Pm*VRP15 was expressed at 1-3 h post-IPTG induction and expressed in the highest level at 2 h post-IPTG induction. Interestingly, no r*Pm*VRP15 band was observed on Western blot membrane after 3 h post-IPTG induction (Figure 9B).

This indicated that r*Pm*VRP15 was a toxic protein or it was unstable, so no full-length *Pm*VRP15 protein band was detected after 3 h IPTG-induction. From Western blotting analysis, most of r*Pm*VRP15 was found in inclusion bodies and only slightly amount of protein was found (Figure 10). This may due to the fact that *Pm*VRP15 contained a transmembrane helical domain.

*3.10 Confirmation of purified rPmVRP15 by Western blot analysis*

Purified r*Pm*VRP15 protein was confirmed by Western blotting analysis. Membrane was incubated with a 1:3,000 dilution of mouse anti-His antibody at 37 °C

for 3 h. After washing with PBST, membrane was incubated in a secondary antibody solution, the alkaline phosphatase-conjugated rabbit anti-mouse IgG, 1:10,000 dilution at RT for 1 hour and detected in darkness with 10 ml of detection buffer (100 mM Tris-HCl, 100 mM NaCl and 50 mM MgCl2, pH 9.5) containing 44 µL of NBT and 33 µL of BCIP as substrate. The protein band of 15 kDa was identified as r*Pm*VRP15 using anti-His antibody (Figure 11).

*3.11 Determination of rPmVRP15 using MALDI-TOF Mass spectrometry (MALDI-TOF MS)*

To determine the molecular weights of r*Pm*VRP15, purified r*Pm*VRP15 was sent to Mahidol University for MALDI-TOF MS analysis. The result showed that molecular mass of r*Pm*VRP15 was 15,899.9 Da (Figure 12).

*3.12 Determination of secondary structure of rPmVRP15 using Circular Dichroism (CD) spectroscopy*

To determine the secondary structure of r*Pm*VRP15, Circular dichroism (CD) spectroscopy was used. CD spectra of r*Pm*VRP15 revealed that the major secondary structure type of r*Pm*VRP15 was alpha-helix (Figure 13), in comparison to standard protein which known secondary structure.

The amount of regular secondary structures (α-helix and ß-strand) were estimated by analysis of the CD spectra using K2D3 deconvolution software (Louis-Jeune et al., 2011). The result showed that the predicted secondary structure percentages of r*Pm*VRP15 was 48.45% α-helix and 13.57% ß-strand (data not shown).

**DISCUSSION**

In previously study, *Pm*VRP15 was identified from SSH libraries of WSSV infected-shrimp (Vatanavicharn et al., 2014). However, *Pm*VRP15 had no significant amino acid sequence similarity to any proteins in the NCBI GenBank database using BLASTX search. From a protein-structural analysis (TMHMM Server v. 2.0) (Krogh et al., 2001), this protein contained a transmembrane helix of 23 amino acids. Localization study showed that *Pm*VRP15 located at nuclear membrane (Vatanavicharn et al., 2014). Based on these evidences, *Pm*VRP15 may function at least in part as a nuclear membrane or related with membrane protein.

In primary hemocyte cultures, *Pm*VRP15 was highly up-regulated after WSSV infection (Figure 3). *Pm*VRP15-silenced hemocytes also showed a reduction of VP28 expression after WSSV infection compared to normal hemocytes (Figure 4). In addition, WSSV-infected hemocyte cells were fractionated into cytoplasmic, membrane, soluble nuclear, chromatin-bound and cytoskeletal fractions and probed with anti-*Pm*VRP15 antibody. The result showed that *Pm*VRP15 was found in soluble nucleus and chromatin-bound fractions (Figure 7). Based on these results, *Pm*VRP15 is a nuclear localized protein which involves in WSSV propagation.

Previous study showed that *Pm*VRP15 transcript was found in heart, hepatopancreas, lymphoid, gill and intestine but *Pm*VRP15 transcript was mainly expressed in the hemocytes in normal shrimp (Vatanavicharn et al., 2014). In shrimp, *Pm*VRP15 mRNA expression was up-regulated in hemocytes at 24, 48 and 72 h after WSSV challenge. *Pm*VRP15 transcript was extremely up-regulated by 9,410.1 fold at 48 h post WSSV infection (Vatanavicharn et al., 2014). Knockdown of *Pm*VRP15 caused a reduction of WSSV propagation in shrimp by 4.17 fold (Figure 5).

Additionally, higher amount of *Pm*VRP15 protein was found in WSSV-infected hemocytes, in comparison to one in uninfected cells. These results imply that *Pm*VRP15 is an important gene in shrimp for WSSV infection. In this study, the silencing of *Pm*VRP15 expression in WSSV-infected *P. monodon* hemocytes cell culture resulted in the reduction of VP28 gene expression as compared to control (GFP). This result is in agreement with *In vivo* study (Vatanavicharn et al., 2014).

Many viruses (e.g. influenza and many animal viruses) have viral envelopes covering their protective protein capsids. The envelopes typically are derived from portions of the host cell membranes (phospholipids and proteins), but include some viral glycoproteins. Functionally, viral envelopes are frequently structural components of the virus that mediate the crucial tasks of receptor recognition and membrane fusion. This occurs by fusion of the envelope with a cellular membrane. The viral envelope then fuses with the host's membrane, allowing the capsid and viral genome to enter and infect the host. Viruses must deliver their genome into the host cells to initiate replication.

Viruses that replicate in the nucleus of nondividing cells with an intact nuclear membrane transfer their genomes through the nuclear pore complex (NPC) into the nucleus. The strategies to target the NPC differ among viruses but invariably involve specific pathways of signaling, endocytosis, access to the cytosol and cytoplasmic transport (Greber, 2002; Meier and Greber, 2003; Ploubidou and Way, 2001; Poranen et al., 2002; Sodeik, 2000). Nuclear import of incoming viral genomes also depends on viral uncoating and in some cases involves an increase of capsid affinity for the NPC (Greber et al., 1994; Whittaker, 2000).

The final steps in the assembly of enveloped viruses occur in the context of a cellular membrane when the nascent particle undergoes a budding reaction that

simultaneously generates the viral envelope and releases the free virion. The cellular membrane can be the plasma membrane, leading to virus release directly to the extracellular space, or an intracellular membrane (e.g. the ER, golgi apparatus or endosomal system), in which case the virions are delivered into intracellular vacuoles. In addition, certain viruses and viruslike particles (VLPs) undergo engenous replication and can shuttle their genomes in and out of the nucleus without going through a complete virus assembly process from which they are released to the extracellular space by a secretory-type mechanism.

The expression of *Pm*VRP15 transcripts and protein were up-regulated in WSSV-infected *P. monodon* hemocytes (Figure 2 and Figure 3). *Pm*VRP15 protein was found in all three types of hemocytes including granular, semigranular and hyaline cells. Hemocytes are the major immune cells of shrimps and play an essential role in both the cellular and humoral immune responses. These suggested that *Pm*VRP15 may have a broad immune based function to response virus. From immunofluorescence result, *Pm*VRP15 protein was expressed in all three types of hemocytes at 48 h post WSSV infection. The expression of *Pm*VRP15 protein was located in nuclear membrane of the cell. It corresponds to protein domain prediction of *Pm*VRP15 which contained a transmembrane helix. In WSSV-infected hemocytes, the silencing of *Pm*VRP15 showed the lower protein expression of VP28 than silencing of GFP (control). Thus, *Pm*VRP15 is an essential protein for WSSV propagation.

It has been reported that WSSV mainly occurs in the nuclei of infected lymphoid cells (Wang et al., 2000). The GCs and SGCs were found in hemolymph as the targets for WSSV infection by a TEM study. However, clusters of developing virions and mature virions were only found in the nucleus of SGCs (Wang et al.,

2002). Even the morphogenesis of WSSV in the infected nucleus of heavily infected SGCs was observed. The nucleus was filled with many empty premature nucleocapsids, most of which were surrounded loosely with an envelope, with both the shell and envelope open at the same end (Wang et al., 2002). Moreover, Propagation of WSSV was investigated in primary ovarian cultures from the kuruma shrimp *Marsupenaeus japonicas* (Maeda et al., 2004). Electron microscope observations clearly showed that the replication of WSSV occurred in nuclei of ovarian cells. Based on these evidence, WSSV replication and assembly within the nucleus are crucial step in WSSV propagation. It was reported that VP35 (nucleocapsid protein of WSSV) contained a nuclear translocation signal which mediate the viral DNA to nucleus of WSSV-infected insect cells for viral replication (Chen et al., 2002). It is possible that WSSV use *Pm*VRP15 for enter or exit from the nucleus. It is common for a virus to use the host machinery for its advantage. For example, *Pm*Rab7 is used in sorting and endocytic trafficking of virus in the host cells (Sritunyalucksana et al., 2006).

*Pm*VRP15 may function in nuclear as a part of membrane protein or related with membrane protein. It is possible that *Pm*VRP15 involves in nuclear import/export of WSSV. To test this hypothesis, ratio of WSSV DNA in nuclear and cytoplasmic fractions of normal and *Pm*VRP15-silenced hemocytes were compared. Knockdown of *Pm*VRP15 resulted in a lower ratio of WSSV copy number in nuclear to cytoplasmic fractions by 9.3 fold, comparison to that of control (Table 2), indicating that *Pm*VRP15 may involve in nuclear entry of WSSV.

Since a protein with transmembrane helice domain is often found to be difficult to crystallize, soluble parts of *Pm*VRP15 were cloned and expressed in *E.*

*coli* C43 (DE3). N-terminal truncated *Pm*VRP15 contained residue 1-112, while C-terminal truncated *Pm*VRP15 consisted of residue 186-414.

Full-length r*Pm*VRP15 was expressed in *E. coli* C43 (DE3). The result showed that r*Pm*VRP15 was expressed at 1-3 h after IPTG induction and expressed in the highest level at 2 h post-IPTG induction (Figure 9). No *Pm*VRP15 band was found after 3 h induction. This suggested that *Pm*VRP15 may be a toxic protein or an unstable protein. In this research, DM (n-decyl-ß-D-maltopyranoside) was used to solubilize r*Pm*VRP15 to ensure it folded correctly. Membrane protein can be solubilize with DM detergent to study their structure and function. Proteins bound to cell membranes have hydrophobic sites buried within the phospholipid bilayers and hydrophilic sites facing toward the water layer. This detergent can interact with the hydrophobic sites of proteins which are then solubilized in the water layer. Moreover, DM detergent does not interfere the bioactivities of target proteins, denature or inactivate target proteins (Prive, 2007). In this study, r*Pm*VRP15 was purified by two steps; Ni-NTA Sepharose™ 6 FF and HiTrap DEAE FF columns, in order to obtain fairly pure protein (Figure 11). Molecular mass of purified r*Pm*VRP15 was determined by MALDI-TOF MS. r*Pm*VRP15 has a molecular mass of 15,899.9 Da (Figure 12), which is similar to the calculated molecular mass.

Furthermore, Circular dichroism (CD) was used to predict secondary structure of r*Pm*VRP15. CD spectroscopy is a powerful method in structural biology to examine the structure and conformational changes of proteins, polypeptides, and peptide structures, which by informing on binding and folding properties provides information about their biological functions. It is based on the dependence of the optical activity of the protein in the far ultraviolet (UV) regions (170–240 nm wavelength) with the backbone orientation of the peptide bonds with minor influences

from the side chains (Farman, 1996). Different types of secondary structure producing characteristic spectra, the spectrum of a given protein can be used to estimate its percentage content on the major secondary structure types (Greenfield, 2006; Kelly et al., 2005).

CD spectra of r*Pm*VRP15 revealed that the major secondary structure type of r*Pm*VRP15 was alpha-helix, compared to standard protein which known secondary structure. The amount of regular secondary structures (α-helix and ß-strand) were estimated by analysis of the CD spectra using K2D3 deconvolution software (Louis-Jeune et al., 2011). The result showed that the predicted secondary structure percentages of r*Pm*VRP15 was 48.45% α-helix and 13.57% ß-strand (data not shown). The fact that purified *Pm*VRP15 adopted secondary structure indicated that the purification procedure used in this study did not destroy protein secondary structure.

**Acknowledgements**

We thank Assoc. Prof. Chartchai Krittanai and his staff at Mahidol University for access to the CD spectrometer. We thank Dr. Sujint Thammasart, D.V.M. at Charoen Pokphand Foods PCL and Mr. Arthit Chalorsrikul, Aquatic Animal Health Research Center CPF for their kind assistance in detection of WSSV copy number. This work was supported by Thailand Research Fund (RSA5580053) and the 90$^{th}$ Year Chulalongkorn Scholarship (to KJ and KK). Additional support came from National Research University Project, Office of Higher Education Commission (WCU-58-013-FW), The Thailand Research Fund through the TRF Senior Research Scholar RTA5580008 (to AT) and IRG 5780008. KJ was supported by His Majesty the King's 72nd Birthday Anniversary Scholarship.

**References**

Aguilar, R.C., Ohno, H., Roche, K.W., Bonifacino, J.S., 1997. Functional domain mapping of the clathrin-associated adaptor medium chains mu1 and mu2. J Biol Chem 272, 27160-27166.

Ahle, S., Mann, A., Eichelsbacher, U., Ungewickell, E., 1988. Structural relationships between clathrin assembly proteins from the Golgi and the plasma membrane. EMBO J 7, 919-929.

Alonso, C., Galindo, I., Cuesta-Geijo, M.A., Cabezas, M., Hernaez, B., Munoz-Moreno, R., 2013. African swine fever virus-cell interactions: from virus entry to cell survival. Virus Res 173, 42-57.

Assavalapsakul, W., Smith, D.R., Panyim, S., 2006. Identification and characterization of a Penaeus monodon lymphoid cell-expressed receptor for the yellow head virus. J Virol 80, 262-269.

Assavalapsakul, W., Tirasophon, W., Panyim, S., 2005. Antiserum to the gp116 glycoprotein of yellow head virus neutralizes infectivity in primary lymphoid organ cells of *Penaeus monodon*. Dis. Aqua. Org. 63, 85-88.

Bartosch, B., Cosset, F.L., 2006. Cell entry of hepatitis C virus. Virology 348, 1-12.

Bernardes, C., Antonio, A., Pedroso de Lima, M.C., Valdeira, M.L., 1998. Cholesterol affects African swine fever virus infection. Biochim Biophys Acta 1393, 19-25.

Blanchard, E., Belouzard, S., Goueslain, L., Wakita, T., Dubuisson, J., Wychowski, C., Rouille, Y., 2006. Hepatitis C virus entry depends on clathrin-mediated endocytosis. J Virol 80, 6964-6972.

Chantanachookin, C.S., Boonyaraypalin, J., Kasornchnadra, S., Direkbusarakorm, U., Ekpanithanpong, K., Supamataya, S., Sriurairatana, T., Flegel, W., 1993. Histologu and ultrastructure reveal a new granulosis-like virus in Penaeus monodon affected by yellowhead disease. Dis. Aqua. Org. 17, 145-157.

Chen, L.L., Leu, J.H., Huang, C.J., Chou, C.M., Chen, S.M., Wang, C.H., Lo, C.F., Kou, G.H., 2002. Identification of a nucleocapsid protein (VP35) gene of shrimp white spot syndrome virus and characterization of the motif important for targeting VP35 to the nuclei of transfected insect cells. Virology 293, 44-53.

Chen, Y., Maguire, T., Hileman, R.E., Fromm, J.R., Esko, J.D., Linhardt, R.J., Marks, R.M., 1997. Dengue virus infectivity depends on envelope protein binding to target cell heparan sulfate. Nat Med 3, 866-871.

Chou, T., 2007. Stochastic entry of enveloped viruses: fusion versus endocytosis. Biophys J 93, 1116-1123.

Chu, J.J., Leong, P.W., Ng, M.L., 2006. Analysis of the endocytic pathway mediating the infectious entry of mosquito-borne flavivirus West Nile into Aedes albopictus mosquito (C6/36) cells. Virology 349, 463-475.

Cole, C., Barber, J.D., Barton, G.J., 2008. The Jpred 3 secondary structure prediction server. Nucleic Acids Res 36, W197-201.

Crowther, R.A., Finch, J.T., Pearse, B.M., 1976. On the structure of coated vesicles. J Mol Biol 103, 785-798.

Diaz-Griffero, F., Jackson, A.P., Brojatsch, J., 2005. Cellular uptake of avian leukosis virus subgroup B is mediated by clathrin. Virology 337, 45-54.

Dimitrov, D.S., 2004. Virus entry: molecular mechanisms and biomedical applications. Nat Rev Microbiol 2, 109-122.

Durand, S., Lightner, D.V., 2002. Quantitative real-time PCR for the measurement of white spot syndrome virus in shrimp. Journal of fish diseases 25, 381-389.

Flegel, T.W., 1997. Special topic review: major viral diseases of the black tiger prawn (*Penaeus monodon*) in Thailand. World Journal of Microbiology & Biotechnology 13, 433-442.

Greber, U.F., 2002. Signalling in viral entry. Cellular and molecular life sciences : CMLS 59, 608-626.

Greber, U.F., Singh, I., Helenius, A., 1994. Mechanisms of virus uncoating. Trends in microbiology 2, 52-56.

Husain, M., Moss, B., 2005. Role of receptor-mediated endocytosis in the formation of vaccinia virus extracellular enveloped particles. J Virol 79, 4080-4089.

Jitrapakdee, S., Unajak, S., Sittidilokratna, N., Hodgson, R.A., Cowley, J.A., Walker, P.J., Panyim, S., Boonsaeng, V., 2003. Identification and analysis of gp116 and gp64 structural glycoproteins of yellow head nidovirus of Penaeus monodon shrimp. J Gen Virol 84, 863-873.

Kim, C., Bergelson, J.M., 2012. Echovirus 7 entry into polarized intestinal epithelial cells requires clathrin and Rab7. MBio 3.

Krogh, A., Larsson, B., von Heijne, G., Sonnhammer, E.L., 2001. Predicting transmembrane protein topology with a hidden Markov model: application to complete genomes. Journal of molecular biology 305, 567-580.

Lightner, D.V., Hasson, K.W., Whiye, B.L., Redman, R.M., 1998. Experimental infection of Western Hemisphere penaeid shrimp with Asian white spot syndrome virus and Asian yellowhead virus. J. Aquat. Anim. Health 10, 271-281.

Limsuwan, C., 1991. Handbook for cultivation of black tiger prawns. Tansetakit, Bangkok, Thailand.

Liu, H., Jiravanichpaisal, P., Soderhall, I., Cerenius, L., Söderhäll, K., 2006. Antilipopolysaccharide factor interferes with white spot syndrome virus replication in vitro and in vivo in the crayfish *Pacifastacus leniusculus*. Journal of virology 80, 10365-10371.

Louis-Jeune, C., Andrade-Navarro, M.A., Perez-Iratxeta, C., 2011. Prediction of protein secondary structure from circular dichroism using theoretically derived spectra. Proteins.

Lu, Y., Tapay, L.M., Brock, J.A., Loh, P.C., 1994. Infection of the yellowhead baculo-like virus (YBV) in two species of penaeid shrimp, Penaeus stylirostris (Simpson) and Penaeus vannamei (Boone). J. Fish. Dis. 17.

Lu, Y., Tapay, L.M., Gose, R.B., Brock, J.A., Loh, P.C., 1997. Infectivity of yellowhead virus (YHV) and the Chinese baculo-like virus (CBV) in two species of penaeid shrimp, Penaeus stylirostris (Stimpson) and Penaeus vannamei (Boone). in: Flegel, F.W., MacRae, I.H. (Eds.), Diseases in Asian Aquaculture III. Asian Fisheries Society, Manila, Philippine.

Lu, Y., Tapay, L.M., Loh, P.C., Brock, J.A., Gose, R.B., 1995. Distribution of yellow head virus in selected tissue and organs of penaeid shrimp Penaeus vannamei. Dis. Aqua. Org. 23, 67-70.

Maeda, M., Saitoh, H., Mizuki, E., Itami, T., Ohba, M., 2004. Replication of white spot syndrome virus in ovarian primary cultures from the kuruma shrimp, Marsupenaeus japonicus. Journal of virological methods 116, 89-94.

Meier, O., Boucke, K., Hammer, S.V., Keller, S., Stidwill, R.P., Hemmi, S., Greber, U.F., 2002. Adenovirus triggers macropinocytosis and endosomal leakage together with its clathrin-mediated uptake. J Cell Biol 158, 1119-1131.

Meier, O., Greber, U.F., 2003. Adenovirus endocytosis. The journal of gene medicine 5, 451-462.

Meier, O., Greber, U.F., 2004. Adenovirus endocytosis. J Gene Med 6 Suppl 1, S152-163.

Mosso, C., Galvan-Mendoza, I.J., Ludert, J.E., del Angel, R.M., 2008. Endocytic pathway followed by dengue virus to infect the mosquito cell line C6/36 HT. Virology 378, 193-199.

Mousavi, S.A., Malerod, L., Berg, T., Kjeken, R., 2004. Clathrin-dependent endocytosis. Biochem J 377, 1-16.

Ongvarrasopone, C., Chanasakulniyom, M., Sritunyalucksana, K., Panyim, S., 2008. Suppression of *Pm*Rab7 by dsRNA inhibits WSSV or YHV infection in shrimp. Marine biotechnology 10, 374-381.

Pearse, B.M., 1975. Coated vesicles from pig brain: purification and biochemical characterization. J Mol Biol 97, 93-98.

Pearse, B.M., 1976. Clathrin: a unique protein associated with intracellular transfer of membrane by coated vesicles. Proc Natl Acad Sci U S A 73, 1255-1259.

Pearse, B.M., 1978. On the structural and functional components of coated vesicles. J Mol Biol 126, 803-812.

Pfaffl, M.W., 2001. A new mathematical model for relative quantification in real-time RT-PCR. Nucleic acids research 29, e45.

Ploubidou, A., Way, M., 2001. Viral transport and the cytoskeleton. Current opinion in cell biology 13, 97-105.

Pongsomboon, S., Tang, S., Boonda, S., Aoki, T., Hirono, I., Tassanakajon, A., 2011. A cDNA microarray approach for analyzing transcriptional changes in *Penaeus monodon* after infection by pathogens. Fish & shellfish immunology 30, 439-446.

Poranen, M.M., Daugelavicius, R., Bamford, D.H., 2002. Common principles in viral entry. Annual review of microbiology 56, 521-538.

Prive, G.G., 2007. Detergents for the stabilization and crystallization of membrane proteins. Methods 41, 388-397.

Rapoport, I., Chen, Y.C., Cupers, P., Shoelson, S.E., Kirchhausen, T., 1998. Dileucine-based sorting signals bind to the beta chain of AP-1 at a site distinct and regulated differently from the tyrosine-based motif-binding site. EMBO J 17, 2148-2155.

Robinson, M.S., 1987. 100-kD coated vesicle proteins: molecular heterogeneity and intracellular distribution studied with monoclonal antibodies. J Cell Biol 104, 887-895.

Simmons, G., Reeves, J.D., Grogan, C.C., Vandenberghe, L.H., Baribaud, F., Whitbeck, J.C., Burke, E., Buchmeier, M.J., Soilleux, E.J., Riley, J.L., Doms, R.W., Bates, P., Pohlmann, S., 2003a. DC-SIGN and DC-SIGNR bind ebola glycoproteins and enhance infection of macrophages and endothelial cells. Virology 305, 115-123.

Simmons, G., Rennekamp, A.J., Chai, N., Vandenberghe, L.H., Riley, J.L., Bates, P., 2003b. Folate receptor alpha and caveolae are not required for Ebola virus glycoprotein-mediated viral infection. J Virol 77, 13433-13438.

Sittidilokratna, N., Dangtip, S., Cowley, J.A., Walker, P.J., 2008. RNA transcription analysis and completion of the genome sequence of yellow head nidovirus. Virus Res 136, 157-165.

Sodeik, B., 2000. Mechanisms of viral transport in the cytoplasm. Trends in microbiology 8, 465-472.

Spann, K.M., Donaldson, R.A., Cowley, J.A., walker, P.J., Lester, R.J.G., 2000. Differences in the susceptibility of some penaeid prawn species to gill-associated virus (GAV) infection. Dis. Aqua. Org. 4, 221-225.

Spann, K.M., McCulloch, R.J., Cowley, J.A., East, I.J., Walker, P.J., 2003. Detection of gill-associated virus (GAV) by in situ hybridization during acute and chronic infections of Penaeus monodon and P. esculentus. Dis. Aqua. Org. 56, 1-10.

Sritunyalucksana, K., Wannapapho, W., Lo, C.F., Flegel, T.W., 2006. *Pm*Rab7 is a VP28-binding protein involved in white spot syndrome virus infection in shrimp. Journal of virology 80, 10734-10742.

Suzuki, T., Takahashi, T., Guo, C.T., Hidari, K.I., Miyamoto, D., Goto, H., Kawaoka, Y., Suzuki, Y., 2005. Sialidase activity of influenza A virus in an endocytic pathway enhances viral replication. J Virol 79, 11705-11715.

Tassaneetrithep, B., Burgess, T.H., Granelli-Piperno, A., Trumpfheller, C., Finke, J., Sun, W., Eller, M.A., Pattanapanyasat, K., Sarasombath, S., Birx, D.L., Steinman, R.M., Schlesinger, S., Marovich, M.A., 2003. DC-SIGN (CD209) mediates dengue virus infection of human dendritic cells. J Exp Med 197, 823-829.

Ungewickell, E., Branton, D., 1981. Assembly units of clathrin coats. Nature 289, 420-422.

Ungewickell, E.J., Hinrichsen, L., 2007. Endocytosis: clathrin-mediated membrane budding. Curr Opin Cell Biol 19, 417-425.

Vatanavicharn, T., Prapavorarat, A., Jaree, P., Somboonwiwat, K., Tassanakajon, A., 2014. *Pm*VRP15, a novel viral responsive protein from the black tiger shrimp, *Penaeus monodon*, promoted white spot syndrome virus replication. PloS one 9, e91930.

Vonderheit, A., Helenius, A., 2005. Rab7 associates with early endosomes to mediate sorting and transport of *Semliki forest* virus to late endosomes. PLoS biology 3, e233.

Walker, P.J., Bonami, J.R., Boonsaeng, V., Chang, P.S., Cowley, J.A., Enjuanes, L., Flegel, T.W., Lightner, D.V., Loh, P.C., Snijder, E.J., Tang, K., 2005. Family roniviridae. Elsevier/Academic Press, London.

Wang, C.H., Yang, H.N., Tang, C.Y., Lu, C.H., Kou, G.H., Lo, C.F., 2000. Ultrastructure of white spot syndrome virus development in primary lymphoid organ cell cultures. Diseases of aquatic organisms 41, 91-104.

Wang, C.S., Tang, K.J., Kuo, G.H., Chen, S.N., 1996. Yellowhead disease-like virus infection in the kuruma shrimp Penaeus japonicus cultured in Taiwan. Fish. Pathol. 31, 177-182.

Wang, Y.T., Liu, W., Seah, J.N., Lam, C.S., Xiang, J.H., Korzh, V., Kwang, J., 2002. White spot syndrome virus (WSSV) infects specific hemocytes of the shrimp *Penaeus merguiensis*. Diseases of aquatic organisms 52, 249-259.

Whittaker, G.R., Kann, M., and Helenius, A. , 2000. Viral entry into the nucleus. . Annu Rev Cell Dev Biol 16, 627-651.

Wijegoonawardane, P.K., Cowley, J.A., Phan, T., Hodgson, R.A., Nielsen, L., Kiatpathomchai, W., Walker, P.J., 2008. Genetic diversity in the yellow head nidovirus complex. Virology 380, 213-225.

Wongteerasupaya, C., Sriurairatana, T., Vickers, J.E., Anutara, A., Boonsaeng, V., Panyim, S., Tassanakajon, A., Withyachumnarnkul, B., Flegel, T.W., 1995. Yellowhead virus of Penaeus monodon is an RNA virus. Dis. Aqua. Org. 22, 45-50.

**Figure legends**

**Figure 1** Experiment hypotheses: (A) *Pm*VRP15 involves in viral entry. (B) *Pm*VRP15 involves in viral exit.

**Figure 2** *Pm*VRP15 mRNA levels in response to WSSV infection. Relative expression ratios of *Pm*VRP15 transcript levels was determined in WSSV-infected *P. monodon* hemocytes by RT-PCR, compared to control (non-infected) shrimp and standardized against elongation factor-1 alpha (EF-1α) as an internal reference, at 0, 6, 12, 24, 48 and 72 h post-WSSV infection.

**Figure 3** Up-regulation of *Pm*VRP15 mRNA in response to WSSV infection. Relative expression ratios of *Pm*VRP15 transcript levels was determined in WSSV-infected *P. monodon* hemocytes by real time RT-PCR, compared to control (non-infected) shrimp and standardized against elongation factor-1 alpha (EF-1 alpha) as the internal reference, at 0, 6, 12, 24, 48 and 72 h post-WSSV infection. The statistical significance of the data was evaluated using one-way ANOVA followed by post hoc test (Duncan's new multiple range test). Data differences were considered significant at $P < 0.01$.

**Figure 4** Silencing of *Pm*VRP15 expression in WSSV-infected *P. monodon* hemocytes resulted in the reduction of VP28 gene expression. RT-PCR analysis of VP28 and *Pm*VRP15 gene of hemocytes shrimp primary cell culture at 24 hour post WSSV injection.

**Figure 5** Silencing of VRP15 mRNA in response to WSSV propagation. Relative expression ratios of VP28 transcription level was determined in WSSV-infected *P. monodon* hemocytes by real time RT-PCR, compared to control (normal WSSV-infected shrimp hemocytes) and standardized against elongation factor-1 alpha (EF-1 alpha) as an internal reference, at 24 h post-WSSV infection. The data represent the mean ($\pm$ 1 SD) relative expression of VP28, derived from three independent experiments. Means with an asterisk are significantly different ($P < 0.01$).

**Figure 6** Immunofluorescent staining analysis of the *Pm*VRP15 protein content in the *Pm*VRP15 silencing of WSSV-infected hemocytes, in comparison to that of control (GFP silencing of WSSV-infected hemocytes) by confocal laser scanning microscopy. Hemocytes from *Pm*VRP15-silenced and GFP-silenced WSSV-infected shrimp at 48 hpi were collected (three individual were pooled) and fixed in 4% paraformadehyde. The fixed 1 x $10^6$ cells/ml of hemocytes were attached to poly-L-lysine coated slides. The *Pm*VRP15 and VP28 were detected using purified rabbit polyclonal anti-*Pm*VRP15 and purified mouse monoclonal anti-VP28, respectively. The hemocytes were then probed with secondary antibodies conjugated with Alexa Flour 488 (green) for *Pm*VRP15, Alexa Flour 568 (red) for VP28 and TO-PRO-3 iodide (adjusted to blue color) for nuclei staining. The GC, SGC and HC are granular, semigranular and hyaline cells, respectively. BFs are bright field images. The scale bar corresponds to 5 μm. Images are representative of 3 fields of view per sample.

**Figure 7** Western blotting analysis of the *Pm*VRP15 protein in WSSV-infected hemocytes. Lane M is a protein marker. Lane 1-5 are cytoplasmic, membrane, soluble nuclear, chromatin-bound and cytoskeletal fraction, respectively.

**Figure 8** Western blot analysis of cytoplasmic and nuclear fractions of WSSV-infected *Pm*VRP15-silenced and GFP-silenced hemocytes using Pierce® Fast Western Blot Kit, SuperSignal® West Femto kit. NPC protein was detected using anti-NPC (Abcam) as primary antibody and Fast Western Mouse Optimized HRP Reagent, Femto as secondary antibody, respectively. X-ray film was developed to observed the signals. Lane 1 is nuclear fractions of WSSV-infected GFP-silenced. Lane 2 is nuclear fractions of WSSV-infected *Pm*VRP15-silenced. Lane 3 is cytoplasmic fractions of WSSV-infected GFP-silenced. Lane 4 is cytoplasmic fractions of WSSV-infected GFP-silenced.

**Figure 9** Expression of r*Pm*VRP15 in *E. coli* C43 (DE3). The r*Pm*VRP15 was expressed in *E. coli* C43 (DE3) and induced with 1 mM IPTG for 0, 1, 2, 3, 4, 5 and 6 hour. Expression of r*Pm*VRP15 was analyzed by 15% SDS-PAGE followed by coomassie brilliant blue staining (A) and Western blotting (B). Lane M is the protein marker.

**Figure 10** Coomassie brilliant blue staining (upper panel) and Western blot analysis (lower panel) of r*Pm*VRP15 in *E. coli* C43 (DE3). (S; soluble fraction, P; pellet or inclusion bodies protein fraction).

**Figure 11** 15% SDS-PAGE followed by coomassie brilliant blue staining (A) and Western blotting (B) analysis of purified r*Pm*VRP15

**Figure 12** MALDI-TOF mass spectrometry analysis of r*Pm*VRP15. Molecular mass of r*Pm*VRP15 was 15,899.9 Da.

**Figure 13** CD spectropolarimeter showed the characteristic spectra of different types of secondary structure (A) and CD spectra of r*Pm*VRP15 (B). The major seconadary structure type of r*Pm*VRP15 was alpha-helix.

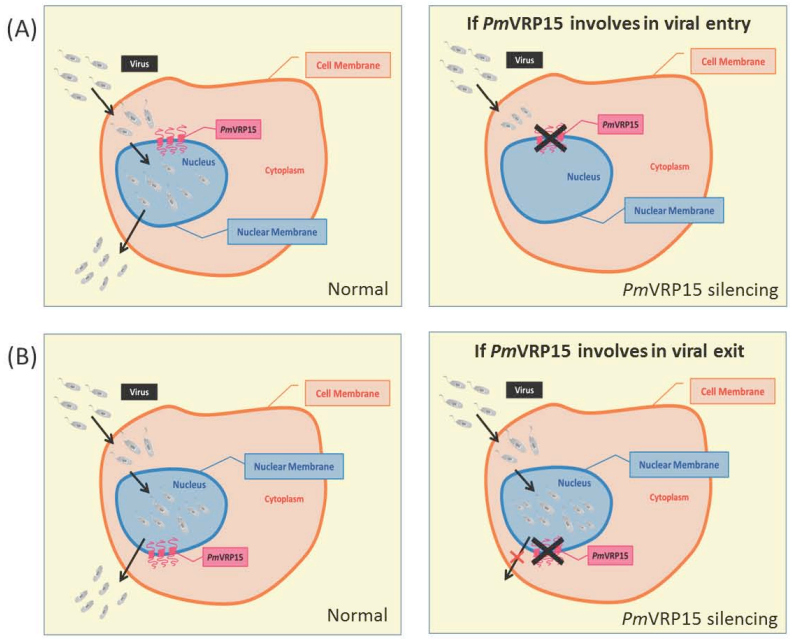


**Figure 1**

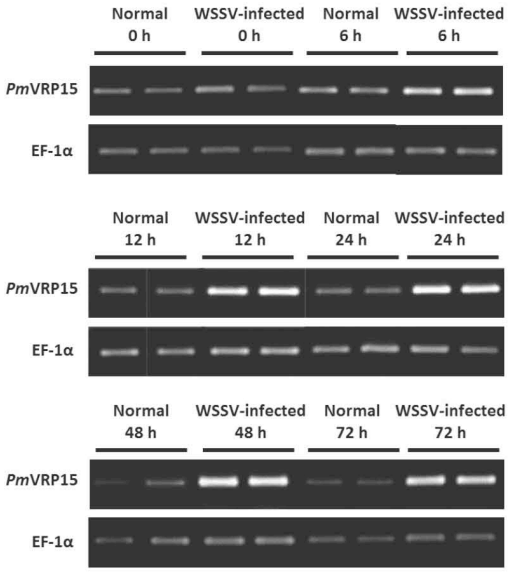


**Figure 2**

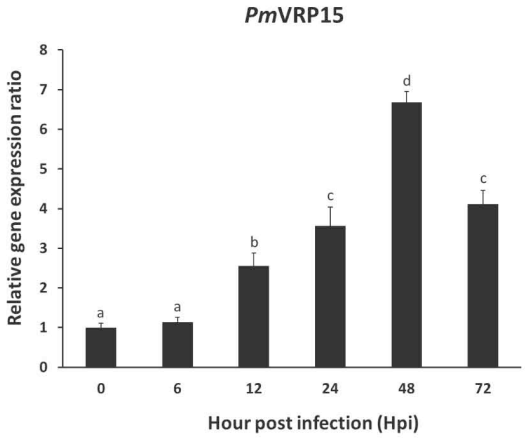


**Figure 3**

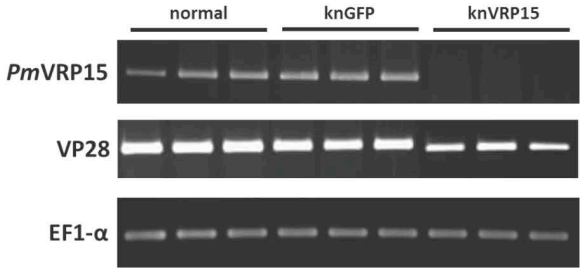


**Figure 4**

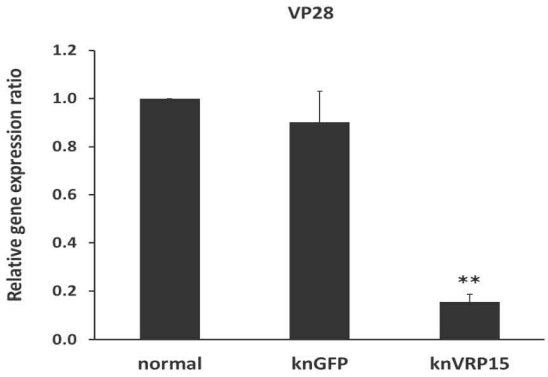


**Figure 5**

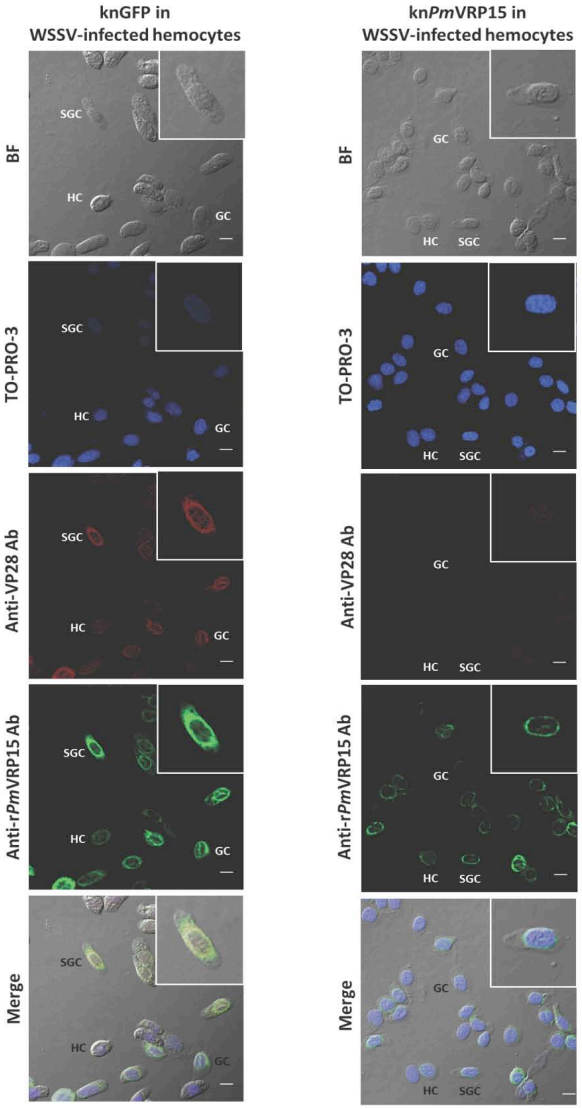
knGFP in
WSSV-infected hemocytes
knPmVRP15 in
WSSV-infected hemocytes
BF
TO-PRO-3
Anti-VP28 Ab
Anti-rPmVRP15 Ab
Merge
SGC
HC
GC

**Figure 6**

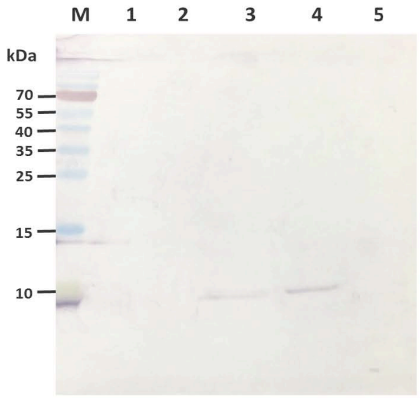


**Figure 7**

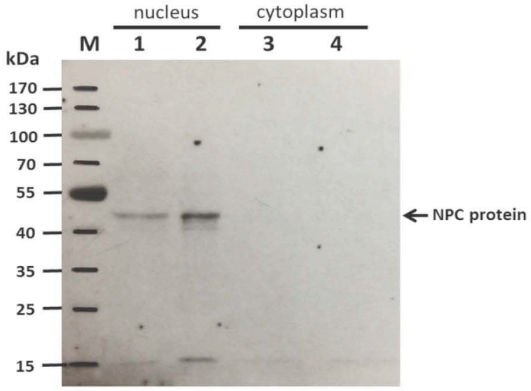


**Figure 8**

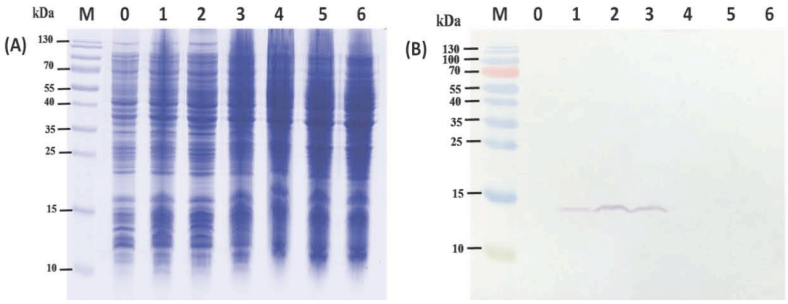


**Figure 9**

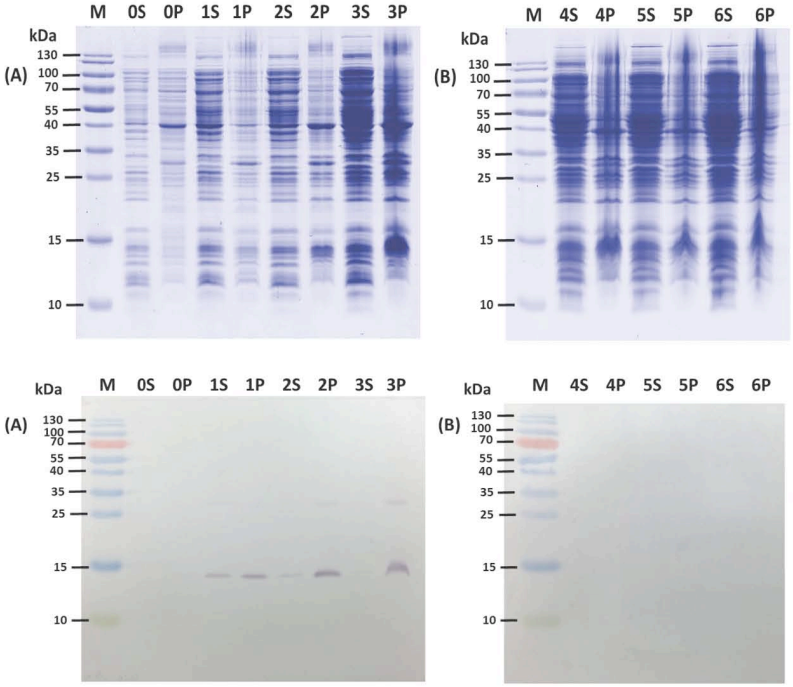


**Figure 10**

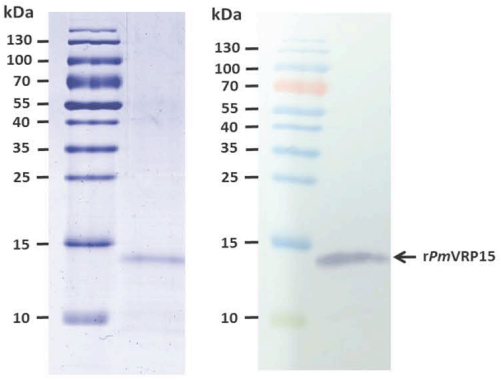


**Figure 11**

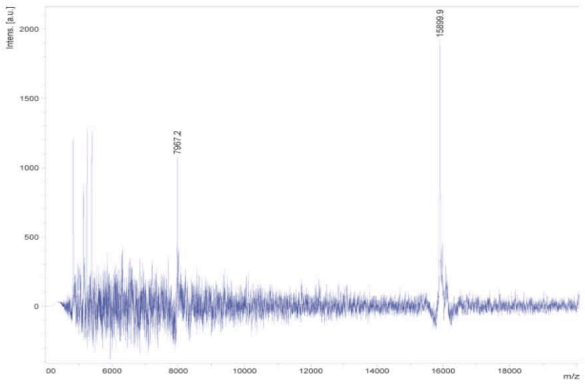


**Figure 12**

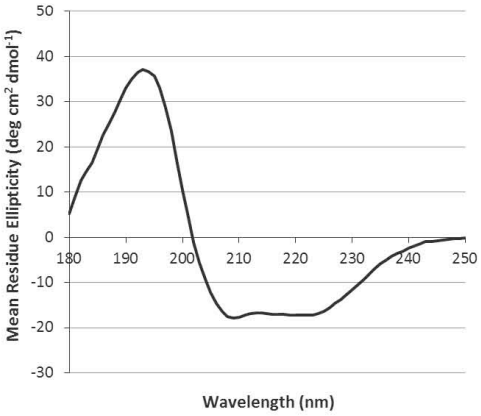


**Figure 13**

**Table 1**

| Primer | Sequence (5′-3′) | Usage |
|---|---|---|
| EF1-α QF | GGTGCTGGACAAGCTGAAGGC | qRT-PCR |
| EF1- α QR | CGTTCCGGTGATCATGTTCTTGATG | qRT-PCR |
| GFP-F | ATGGTGAGCAAGGGCGAGGA | dsRNA synthesis |
| GFP-R | AGAAGGAAGGGCGCTGAC | dsRNA synthesis |
| VP28-FRT | TCACTCTTTCGGTCGTGTCG | RT-PCR |
| VP28-RRT | CCACACACAAAGGTGCCAAC | RT-PCR |
| VP28QF | GGGAACATTCAAGGTGTGGA | qRT-PCR |
| VP28QR | GGTGAAGGAGGAGGTGTTGG | qRT-PCR |
| *Pm*VRP15-1F RNAi | GGATCCTAATACGACTCACTATAGGCGCGA CCGAGCCAAGAGAACAT | dsRNA synthesis |
| *Pm*VRP15-1R RNAi | TGAGCTGACGGAAGGCCACAGA | dsRNA synthesis |
| *Pm*VRP15-2F RNAi | CGCGACCGAGCCAAGAGAACAT | dsRNA synthesis |
| *Pm*VRP15-2R RNAi | GGATCCTAATACGACTCAC TATAGGTGAGCTGACGGAAGGCCACAGA | dsRNA synthesis |
| *Pm*VRP15-QF | CGTCCTTCAGTGCGCTTCCATA | qRT-PCR |
| *Pm*VRP15-QR | ACAGCGACTCCAAGGTCTACGA | qRT-PCR |
| *Pm*VRP15-RTF | CGATCACCACTCTCGTTCTT | RT-PCR |
| *Pm*VRP15-RTR | ACAGCGACTCCAAGGTCTACGA | RT-PCR |
| WSSV1011F | TGGTCCCGTCCTCATCTCAG | WSSV copy number detection |
| WSSV1079R | GCTGCCTTGCCGGAAATTA | WSSV copy number detection |

**Table 2**

| Sample | WSSV in Cytoplasm | WSSV in Nucleus | Average (Nucleus) | Ratio of WSSV in Nucleus/Cytoplasm | Means | Fold |
|---|---|---|---|---|---|---|
| knGFP | 3.83E-03 | 3.92E-02 | 3.82E-02 | 9.97E+00 | 1.11E+01 | |
| | 2.95E-03 | 3.49E-02 | | 1.29E+01 | | |
| | 3.64E-03 | 4.04E-02 | | 1.05E+01 | | |
| kn*Pm*VRP15 | 1.60E-02 | 2.72E-02 | 1.88E-02 | 1.17E+00 | 1.20E+00 | **9.28E+00** |
| | 1.47E-02 | 1.28E-02 | | 1.27E+00 | | |
| | 1.63E-02 | 1.62E-02 | | 1.15E+00 | | |